Incision and channel morphology across active structures along the Peikang River, central Taiwan: Implications for the importance of channel width

Brian J. Yanites[1,†], Gregory E. Tucker[2], Karl J. Mueller[1], Yue-Gau Chen[3], Tarka Wilcox[1], Shao-Yi Huang[3], and Kuo-Wei Shi[3]

[1]*Department of Geological Sciences, University of Colorado, 2200 Colorado Avenue, Boulder, Colorado 80309, USA*
[2]*Cooperative Institute for Research in Environmental Sciences and Department of Geological Sciences, University of Colorado, 2200 Colorado Avenue, Boulder, Colorado 80309, USA*
[3]*Department of Geosciences, National Taiwan University, No. 1, Sec. 4th, Roosevelt Road, Taipei 106, Taiwan, Republic of China*

ABSTRACT

River morphology and dynamics are strongly influenced by active tectonics. We report channel dynamics for the Peikang River, which flows through the Hsuehshan Range in central Taiwan. Using a digital elevation model and field surveys, we constrain channel morphology for an ~90 km stretch of river to calculate unit stream power and boundary shear stress along the river path. Incision rates are estimated with optically stimulated luminescence dating of sand deposited on strath terraces. We find a strong correlation between unit stream power/shear stress and incision rate, but only if variation in channel width is considered. A calibrated river incision rule implies river incision rates of ~9–13.5 mm/yr upstream of the Meiyuan and Tili faults and suggests that one or both of these structures are presently active. Our results indicate that the Shuilikeng fault is also actively deforming, as incision rates increase to ~6–10 mm/yr across it, compared to 1–4 mm/yr in adjacent reaches. Prominent narrowing across the Shuilikeng fault, and the absence of significant gradient variation indicate that channel width is a first-order morphological adjustment to differential incision. Only when the channel width-to-depth ratio reaches a minimum does the channel slope significantly adjust to local changes in base level, as is the case upstream of the Meiyuan and Tili faults.

INTRODUCTION

Analysis of stream morphology has proven valuable for mapping differential rock uplift relative to a fixed datum such as the geoid (Pazzaglia and Brandon, 2001; Kirby and Whipple, 2001; Lave and Avouac, 2001; Whipple and Tucker, 1999; Wobus et al., 2006a). The approach builds upon the idea that channel morphology mirrors the erosion rate of the stream (Howard and Kerby, 1983). In areas where channel incision roughly balances the rate of rock uplift, spatial variations in channel morphology (after properly accounting for factors such as drainage area and lithology) indicate corresponding variations in rock-uplift rate. Full realization of the potential of this method requires a deeper understanding of how and why channels adjust to differential rock uplift. To help illuminate the dynamics of a channel flowing over zones of differential rock uplift, we have documented channel morphology and incision rate for a river crossing a number of thrust faults in central Taiwan. We focus on this region because it represents a natural experiment in bedrock incision where differential rock uplift associated with active slip on an array of thrust faults occurs in response to ~40 mm/yr of crustal shortening (Simoes and Avouac, 2006). By quantifying the relationship between channel morphology and incision rate for a river crossing a number of these faults, we seek to add to the growing data set that characterizes patterns of Holocene strain in west-central Taiwan.

Rivers serve as efficient conduits for water traversing a potential energy gradient. As water flows through these conduits, it loses potential energy. Most of a river's potential energy is expended as heat and work, and some of the latter drives sediment transport and erosion of bedrock. For example, energy can be transferred to saltating bed load, which can impact, fracture, and abrade exposed bedrock; it can be dissipated via turbulent eddies that can come in contact with bedrock and scour it with suspended particles; it can produce pressure fluctuations that act to lift bedrock and sediment from the bed; or it can exert a shear traction that will slide blocks or pieces of bedrock out of the rock mass or rotate sediment out of place (Whipple et al., 2000). A growing body of literature uses unit stream power (or the rate of energy loss per unit area of the riverbed) and boundary shear stress as proxies for the rate of these erosion processes (Howard and Kerby, 1983; Hancock et al., 1998; Kirby et al., 2003; Lave and Avouac, 2001; Roe et al., 2006; Snyder et al., 2000; Tucker, 2004; Whipple, 2004; Whipple and Meade, 2006; Whipple and Tucker, 1999; Willett, 1999). The magnitude of these hydraulic metrics is a function of two basic morphological parameters of the channel: (1) river slope, which controls the rate at which potential energy is lost, and (2) channel width, which can be considered as a focusing mechanism because it governs the area of bedrock over which the energy is dissipated. It follows that if unit stream power and shear stress are valid proxies for incision rate, and if river incision rate keeps pace with rock-uplift rate, then spatial variations in channel width and slope can indicate where active deformation is occurring.

We mapped the channel morphology and estimated incision rates along the Peikang River in central Taiwan to answer the following set of questions: (1) What are the Holocene rates of incision, and how do they vary downstream? (2) Do along-stream variations in incision rate

[†]E-mail: brian.yanites@colorado.edu

GSA Bulletin; July/August 2010; v. 122; no. 7/8; p. 1192–1208; doi: 10.1130/B30035.1; 11 figures; 2 tables; Data Repository item 2010054.

For permission to copy, contact editing@geosociety.org
© 2010 Geological Society of America

correlate with known faults? (3) Do the incision rates vary systematically with unit stream power or shear stress? (4) Are there systematic variations in lithology that might account for observed patterns? (5) To what degree are variations in unit stream power and/or shear stress linked to variations of width versus slope, and what does this reveal about mechanisms of channel adjustment?

BACKGROUND

Taiwan

The Island of Taiwan results from an arc-continent collision between the Philippine Sea and Eurasian plates (Fig. 1). The resulting thrust belt has evolved from a subaqueous accretionary wedge into a rapidly eroding pair of oppositely verging thrust belts. Our study is limited to the frontal portion of the west-vergent part of the orogen, the so called "pro-wedge" (Willett et al., 1993). The west-vergent thrust belt has been described as a quintessential example of a critical wedge (Suppe, 2007) in which tectonic and surficial processes are balanced to produce a steady-state system with respect to mass fluxes and gross topographic morphology (Dahlen and Suppe, 1988; Willett and Brandon, 2002).

When only considering the mechanical strength of the deforming lithosphere, this balance results in an analytically predictable critical taper angle between the topographic slope and décollement, or main detachment fault. It has been proposed that in order to maintain the balance between mass coming into the orogen through tectonic processes and erosion exporting mass out, the topographic slope on the western side of the island is likely maintained by both tectonic underplating and a series of west-verging thrust sheets that accommodate horizontal shortening (Chen et al., 2007; Simoes et al., 2007b, 2007c; Yue et al., 2005). The mass added to a deforming wedge through these processes also occurs partly in response to erosion, which produces sediment that leaves the orogen via river transport (Dahlen and Barr, 1989; Fuller et al., 2006; Simoes et al., 2007a). Although almost all of the proposed models account for material flux into the orogen through both frontal accretion and underplating, the magnitude and location of the latter process remain under debate (Fuller et al., 2006; Simoes and Avouac, 2006; Simoes et al., 2007a; Yue et al., 2005). A better understanding of the modern-day deformation field will help guide the development of future kinematic and tectonic models for this compressive orogen.

Thrust faults on the western side of the island constitute a major piece of the tectonic framework across the collisional plate margin. The rates and styles of deformation along the two westernmost thrust faults, the Changhua and Chelungpu (Fig. 1), have been fairly well studied, and they (1) deform well-dated synorogenic strata, the age and stratigraphic growth

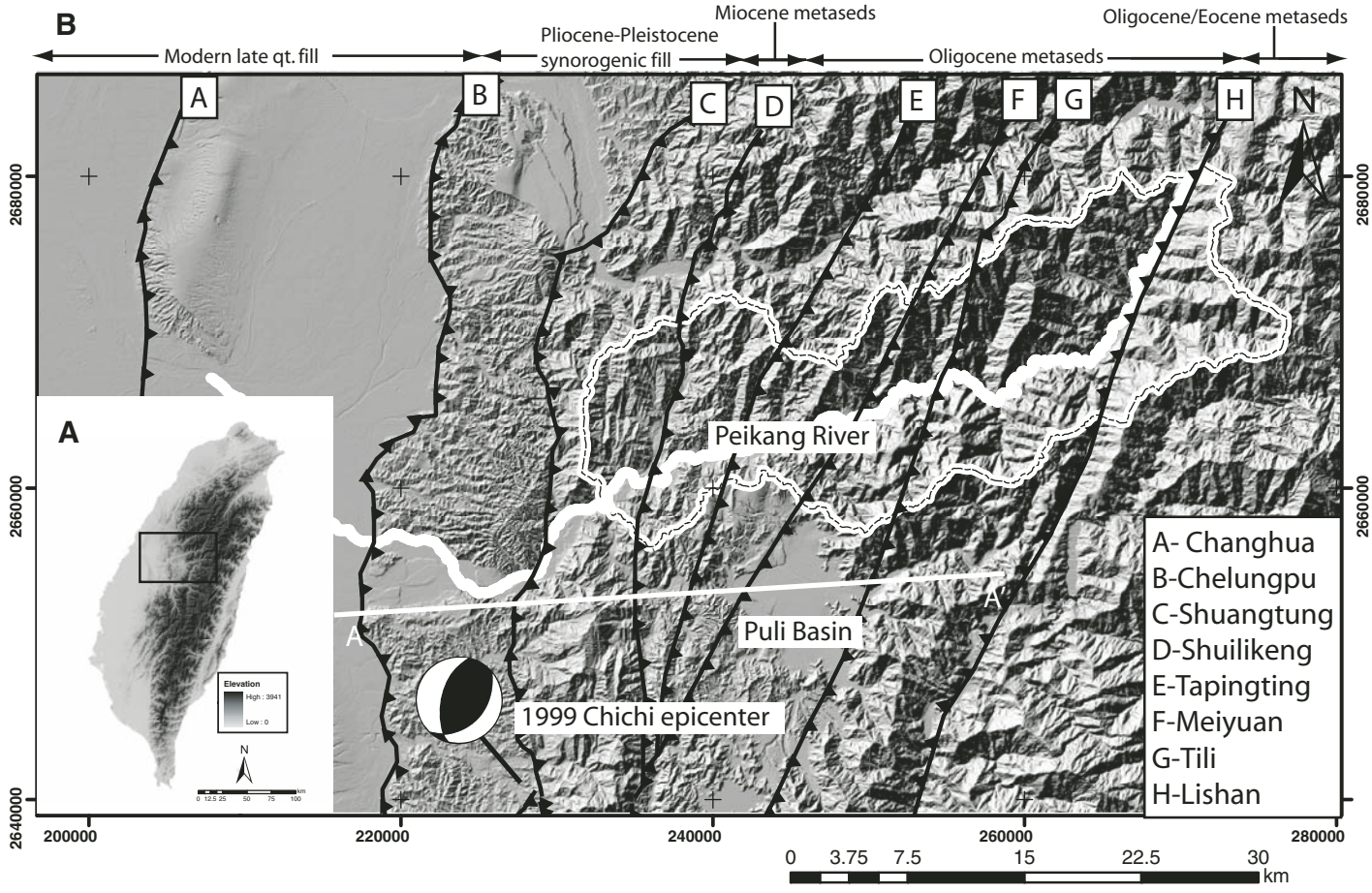

Figure 1. Overview of study area. (A) Hillshade overlaid with a digital elevation model (DEM) for the Island of Taiwan. Black box outlines extent of B. (B) Hillshade and basic geologic map of the study area. West-verging faults and geologic units are taken from Powell (2003). Lithologic boundaries at the top of B define location of the boundaries along the top of the hillshade image. These boundaries follow the faults across the river. Location of cross-section A-A′ in Figure 11 is shown.

architecture of which constrain fault kinematics (Simoes et al., 2007b); (2) have active deposition in the footwall block (Chen et al., 2004; Lee et al., 2001); and (3) have been monitored by a network of continuous global positioning system (GPS) data (Johnson et al., 2001). Relatively less is known about potentially active thrust faults further east, such as the Shuangtung, Shuilikeng, Meiyuan, and Tili faults (Fig. 1; Powell, 2003), in part because these faults (1) have less-well-preserved geomorphic features across the structures, (2) are actively eroding across both their footwall and hanging-wall blocks, and (3) are monitored by fewer permanent GPS base stations. These faults, however, likely play a fundamental role in maintaining wedge taper in this region and account for at least some of the horizontal shortening (Mueller et al., 2001; Powell, 2003; Wilcox et al., 2007). Our analysis of channel morphology thus helps to constrain the modern strain field in the Hsuehshan Range by identifying active structures.

Peikang River

Located just to the north of the Puli Basin in western Taiwan (Fig. 1B), the Peikang River flows almost perpendicular to the structural trend on the island. Unlike other rivers that flow through the Puli Basin, the Peikang is bedrock-lined throughout (i.e., it has to erode bedrock to significantly lower its bed elevation or to widen its banks) and is undammed, making it a suitable river to investigate channel dynamics in response to active deformation in this region of Taiwan. The river headwaters are located in the Eocene-Oligocene metasedimentary rocks of the Lishan valley, formed by the east-verging Lishan thrust (Fig. 1). After flowing ~20 km along the (longitudinal) Lishan Valley, the river valley narrows and sharply turns to the west, crossing the structural grain of the island and flowing over Oligocene metasedimentary rocks. Almost immediately downstream of the Meiyuan fault (~44 km downstream of its headwaters), the river valley abruptly widens, and ubiquitous strath terraces line the valley bottoms. The straths are discontinuous but present throughout. Downstream of the Shuangtung fault (~km 75), the underlying bedrock is composed of soft synorogenic fill, making this reach unsuitable for comparison with upstream reaches. Because the river terraces between the Meiyuan and Shuangtung faults are very discontinuous, often only extending for a few hundred meters along the flow path, we turn to channel morphology and dynamics to pinpoint in more detail whether and where deformation is occurring.

Channel Morphodynamics

Slope-Area Analysis

Empirical evidence shows a strong relationship between channel slope, S, and contributing drainage area, A, for many river basins (Hack, 1957):

$$S = k_s A^{-\theta}, \quad (1)$$

where the concavity, θ, usually is around 0.5 (e.g., Flint, 1974; Tarboton et al., 1989; Tucker and Whipple, 2002). By plotting channel slope and drainage area in log-log space, values of k_s (intercept) and θ (graph slope) can be found for the entire basin (Fig. 2A). If we divide local estimates of slope by the contributing drainage area raised to the –θ power, we find a metric of relative channel steepness, k_s. This factor, often referred to as a steepness index, can then be mapped along the channel flow path to search for strong spatial variations in channel steepness (relative to contributing drainage area). It has been suggested, on both empirical and theoretical grounds, that these variations represent differences in rock-uplift rate for a steady-state river (one in which the vertical rate of incision equals the rate of rock uplift), assuming a uniform climate and lithology (Whipple and Tucker, 1999). We point the reader to Wobus et al. (2006a) for a more thorough explanation of this method. In these approaches, it is often assumed that channel width scales with contributing drainage area and is not considered as an independent variable that can influence the erosive potential of a river.

Unit Stream Power and Shear Stress

A more direct method of using channel morphology as an indicator of active deformation is to explicitly calculate and map unit stream power and/or boundary shear stress. Since these hydraulic metrics are often used as proxies for incision rate, their variation should reflect changes in relative rock-uplift rate in a steady-state river system. Further, calibration of the relationship between these metrics and the rate of incision allows one to quantitatively map rock-uplift rate where actual constraints are unavailable.

Since erosion driven by fluvial processes is a threshold process (Snyder et al., 2003; Tucker, 2004), one can hypothesize that the rate of lowering, E, is proportional to the excess unit stream power, ω, such that

$$E = \begin{cases} k_\omega(\omega - \omega_c) & \omega > \omega_c \\ 0 & \omega \le \omega_c \end{cases}, \quad (2)$$

or to the excess boundary shear stress, τ_b, such that

$$E = \begin{cases} k_\tau(\tau_b - \tau_c) & \tau_b > \tau_c \\ 0 & \tau_b \le \tau_c \end{cases}, \quad (3)$$

where k_ω and k_τ are scaling coefficients that currently must be calibrated for specific climates and lithologies, and ω_c and τ_c are the critical values for incision.

Unit stream power is defined as the rate at which energy is dissipated by the flow per unit area of the river bed. Assuming steady, uniform flow, unit stream power can be calculated from

$$\omega = \rho g \frac{Q_w}{W} S, \quad (4)$$

where ρ is the density of water, g is the gravitational acceleration, Q_w is water discharge, and W is channel width. It is often assumed that discharge is related to contributing drainage area through a runoff coefficient, R,

$$Q_w = RA^c. \quad (5)$$

Shear stress, which for steady, uniform flow equals the slope-parallel weight of the flowing water per unit area, is also a function of cross-section channel geometry. Assuming that channel width is much greater than channel depth, then the shear stress can also be written in terms of discharge, width, and slope,

$$\tau_b = \rho g \left(\frac{n Q_w}{W} \right)^{\frac{3}{5}} S^{\frac{7}{10}}, \quad (6)$$

where n is the Manning friction factor (dimensions [=] $T/L^{1/3}$). Equations 4 and 6 indicate that hydraulic energy dissipation and stress depend on both the gradient and the width of the channel; variations in either or both of these can potentially influence the incision rate (Finnegan et al., 2005; Lave and Avouac, 2001; Whittaker et al., 2007).

The next section explains how we calculate channel slope, width, and water discharge for use in unit stream power and shear stress calculations. These values are then compared to incision rates to test whether either shear stress or unit stream power is an appropriate proxy for incision rate and to decipher the morphological variable (or combination of) that best correlates with observed variations in incision rate for the Peikang River in central Taiwan. Finally, these results are used to constrain rates of erosion in reaches with a paucity of strath terraces.

METHODS

Channel Morphology

We used a combination of digital elevation model (DEM) analysis and field work to constrain channel morphology. Slope was extracted

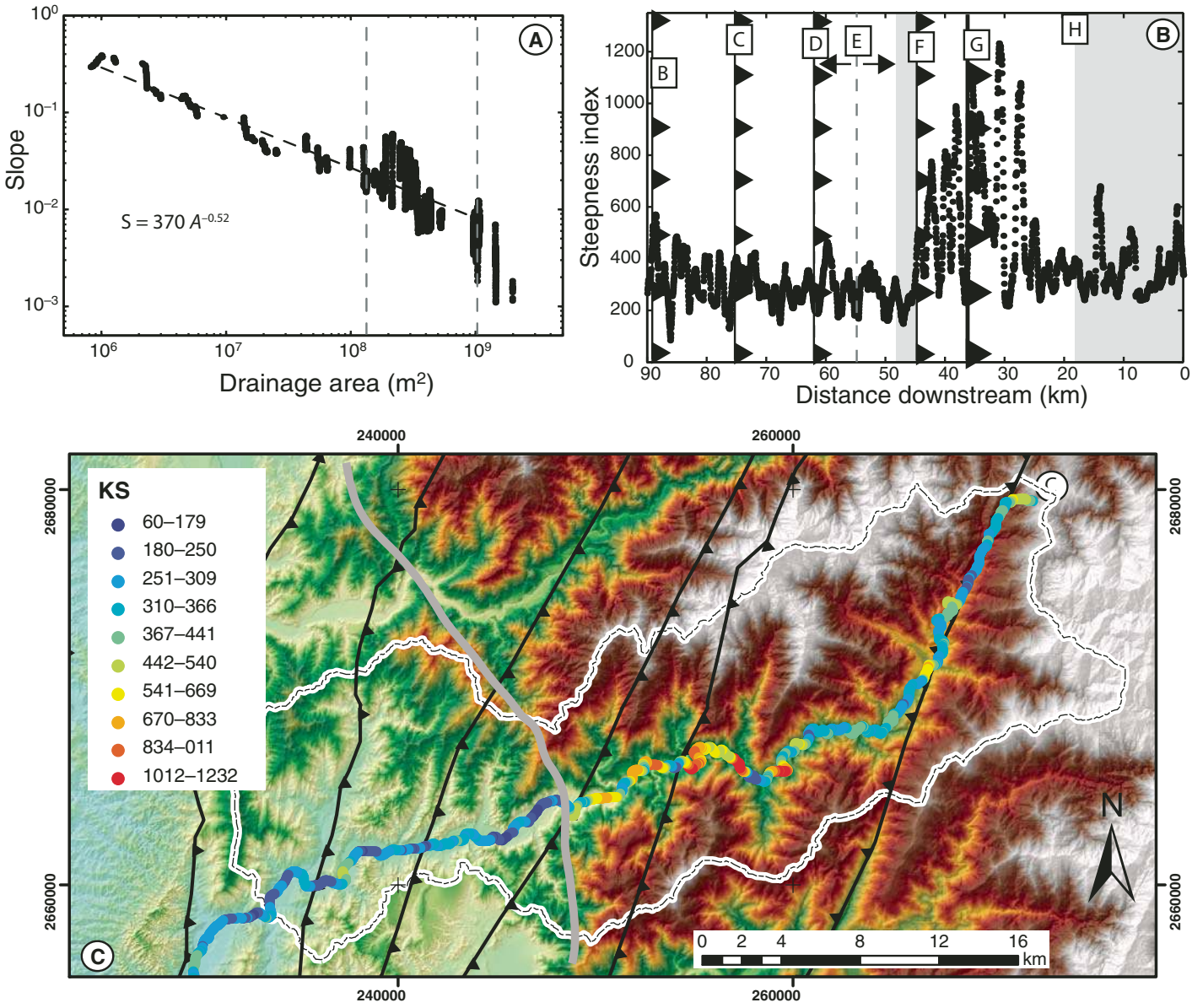

Figure 2. Calculation of steepness indices for the Peikang River. (A) Channel slope and drainage area plotted in log-log space. Regression of data is shown with dotted line and equation. (B) Steepness index, k_s, plotted along the river path. Faults are labeled as in Figure 1B. (C) Steepness indices plotted in map space. For both B and C, note the strong steepness contrast across the Meiyuan fault. The upstream extent of this signal is at river kilometer 28. Gray line in C denotes approximate location of a major physiographic transition in the region that corresponds with this strong steepness signal.

from a 20 m DEM and smoothed over a 1 km window to reduce inherent noise. Channel width was measured perpendicular to the channel flow direction on a hillshade image of the 20 m DEM (Table DR1[1]) and in the field (Table DR2 [see footnote 1]). For the DEM analysis, the left and right banks were delineated by hand along the edge of appropriate bounding terraces. Where no terraces were present, the bank location was estimated at an elevation comparable to bankfull flow depth, which was aided by field observations, and the pixel nearest that elevation was used as the bank. Measurements between the delineated banks, oriented perpendicular to the flow direction, were then made at an average of every 100 m, adjusting the intervals to obtain representative values along a given reach (for example, when width was changing rapidly, we increased the frequency of width estimates). Width was smoothed by averaging any measurements within 250 m upstream and downstream of the point. For areas in which channel width was less than three pixels wide (<60 m), we relied purely on field measurements to estimate channel width. Indicators of recent high flow levels were frequently only 1 m or so below the inner terrace level. Given the rectangular geometry of the channel, it is clear that they represent

[1]GSA Data Repository item 2010054, details related to channel morphology, optically stimulated luminescence (OSL) ages, and lithology, is available at http://www.geosociety.org/pubs/ft2010.htm or by request to editing@geosociety.org.

bankfull flow depth to within a meter. Examples of indictors of high flow include banks scoured of vegetation, freshly abraded bedrock, and discoloration of bedrock. These indicators were then used to measure channel depth at a particular point. Channel cross-section profiles were measured with a handheld laser rangefinder, and bankfull width was estimated at the flood depth elevation. Locations where the field survey and DEM mapping overlapped allowed us to cross check the consistency of the methods, and the close correlation between field and remotely mapped channel width gives us confidence that our methods yield robust results.

Discharge

Estimating discharge, Q_w, in Taiwan is facilitated by a dense network of river stage and precipitation monitoring stations. Daily records of precipitation and discharge extend back to the 1930s for the Peikang River (http://gweb.wra.gov.tw/wrwebeng/). Additionally, hourly precipitation and discharge data for large events date back to the 1970s. One current and three former gauging stations lie within our study reach. To choose a baseline discharge, we analyzed daily and hourly records for large flood events in this river basin. In early July 2004, typhoon Mindulle struck the central part of Taiwan, producing intense rainfall in the Peikang River basin. Rainfall accumulation of over 1 m in a 3 d period produced very high discharges over these three days: average daily discharge values for July 3, 4, and 5 were 1808, 1185, and 1376 m^3/s, respectively (station 1430H032, Fig. 2). The maximum discharge recorded in 1 h intervals for this event was 3914 m^3/s. The same stations recorded another event on 25 August of the same year with a daily discharge of 1295 m^3/s. An event in 1976 produced a daily discharge of 1510 m^3/s. Before 1976, a gauging station located 6.9 km upstream (1430H001) fills in the record back to 1958 and reveals another big event in 1966 that generated a mean daily discharge of 1290 m^3/s. Since no major tributary exists between these stations, it is likely that station 1430H032 had only a slightly higher discharge. Analysis of maximum hourly discharge records over a 19 yr period suggests that the 10 yr flood at station 1430H032 is ~1000 m^3/s. We therefore chose a discharge of 1000 m^3/s at the drainage area of this gauging station as a representative flood. The specific value of discharge is not critical to our analysis because it will not significantly influence the spatial pattern of shear stress and unit stream power. It simply provides the magnitude of shear stress and unit stream power for a 10 yr flood along this river.

Incision Rate

Numerous discontinuous terraces line the Peikang River downstream of the Meiyuan fault (Fig. 3A). These bedrock strath terraces are often capped with 2–5 m of imbricated gravel and conglomerate channel deposits. Unfortunately, soils are too poorly developed and inherently variable (with respect to grain size and outcrop access) to allow creation of a dependable soil chronosequence to correlate terraces upstream and downstream, but the rare sandy lenses within the coarse debris allowed the use of optically stimulated luminescence (OSL) dating techniques to constrain the age of former channel bed elevations. Samples were collected using basic OSL sampling procedures: (1) to avoid bioturbation, only sandy, quartz-bearing units >1 m below the ground surface were sampled; (2) at least 10 cm (usually much more) of the face of the outcrop were removed before sampling; (3) an ~5-cm-diameter polyvinyl chloride (PVC) tube was hammered into the middle of the sandy unit; and (4) the ends were capped and empty space filled with heavy plastic bags. Samples were prepared and run at the Oxford Luminescence Laboratory and the U.S. Geological Survey (USGS) Luminescence Dating Laboratory using standard single aliquot regenerative dose methods (Murray and Wintle, 2000).

The potential for incomplete resetting of sand grains in fluvial deposits requires an analysis of the individual aliquot ages to appropriately choose an age model. Because of the likelihood of incomplete resetting in fluvial environments (Arnold et al., 2007; Wallinga, 2002), and because the distributions of the measured aliquot data met the criteria for partial bleaching suggested by Arnold et al. (2007), we calculated the sample age using the minimum age model for all samples (Galbraith et al., 1999). The minimum age model essentially assumes that some of the grains are not fully reset and others are reset and uses statistical techniques to "find" the measurements from the fully reset grains and calculate an age from those grains and not the partially bleached grains. As an upper bound on the ages, we also calculated ages using the central age model, which assumes that the entire sample is reset.

The OSL samples come from fluvial deposits on top of the strath terraces, recording former channel positions; however, it is important to correct for the depth to bedrock below the sample to accurately record the vertical bedrock incision that occurred after the channel sediment was deposited (Fig. 3B). The depth of post-strath bedrock incision was calculated as the difference between the height of the bedrock-alluvial contact on the terrace (at the sample location) and the estimated height of bedrock in the modern channel. Where bedrock was not visible in the modern channel floor due to the evacuation of sediment following the Chi-Chi earthquake, the depth to bedrock was determined using electrical resistivity surveys (Yanites et al., 2008). The corrections give us a bedrock-to-bedrock depth of incision since the sediments were deposited.

Lithologic Influence

The amount of erosion accomplished for a given unit stream power or shear stress can be influenced by lithology (in other words, lithology influences the value of k in Equations 2 and 3). Thus, it is important to assess the extent to which spatial variations in unit stream power and shear stress might arise from variations in lithology. Our study area is located mostly in the Eocene-Oligocene age metasedimentary rocks of the Hsuehshan Range. Three lithologic formations make up this section. The youngest, the Shuilchangliu Formation, is composed of thickly bedded shale and argillite with thin sandstone beds. The Paileng Formation is a quartzitic sandstone with interbedded argillite, and the oldest, the Chiayang Formation, is mapped as a weakly metamorphosed slate with thin alternations of sandstone and siltstone (Powell, 2003). Toward the downstream end, between the Shuilikeng and Shuangtung faults (Fig. 1), the river flows over Miocene metasedimentary rocks, which are mapped as interbedded shales and sandstones. Downstream of the Shuangtung fault, the river is set in Pliocene-Pleistocene synorogenic fill of the Toukoshan and Cholan Formations, which precludes us from comparing it to the hard bedrock reaches upstream. To test for potential lithology effects along the bedrock reach, we used a proxy for the compressive strength of the mapped units using a concrete test hammer (Schmidt hammer). We recorded more than 25 Schmidt hammer rebound values, correcting for impact angle, at each of 49 locations along the flow path (Fig. 4). Where multiple interbedded lithologies were present, we performed separate tests on the different beds. The mean, median, and standard deviation at each location were calculated to test for major changes along the river path. Further, we estimated the spacing and width of joints, which could also influence the susceptibility to erosion as smaller spacing or wider joints will produce more easily removable blocks of rock (Selby, 1980).

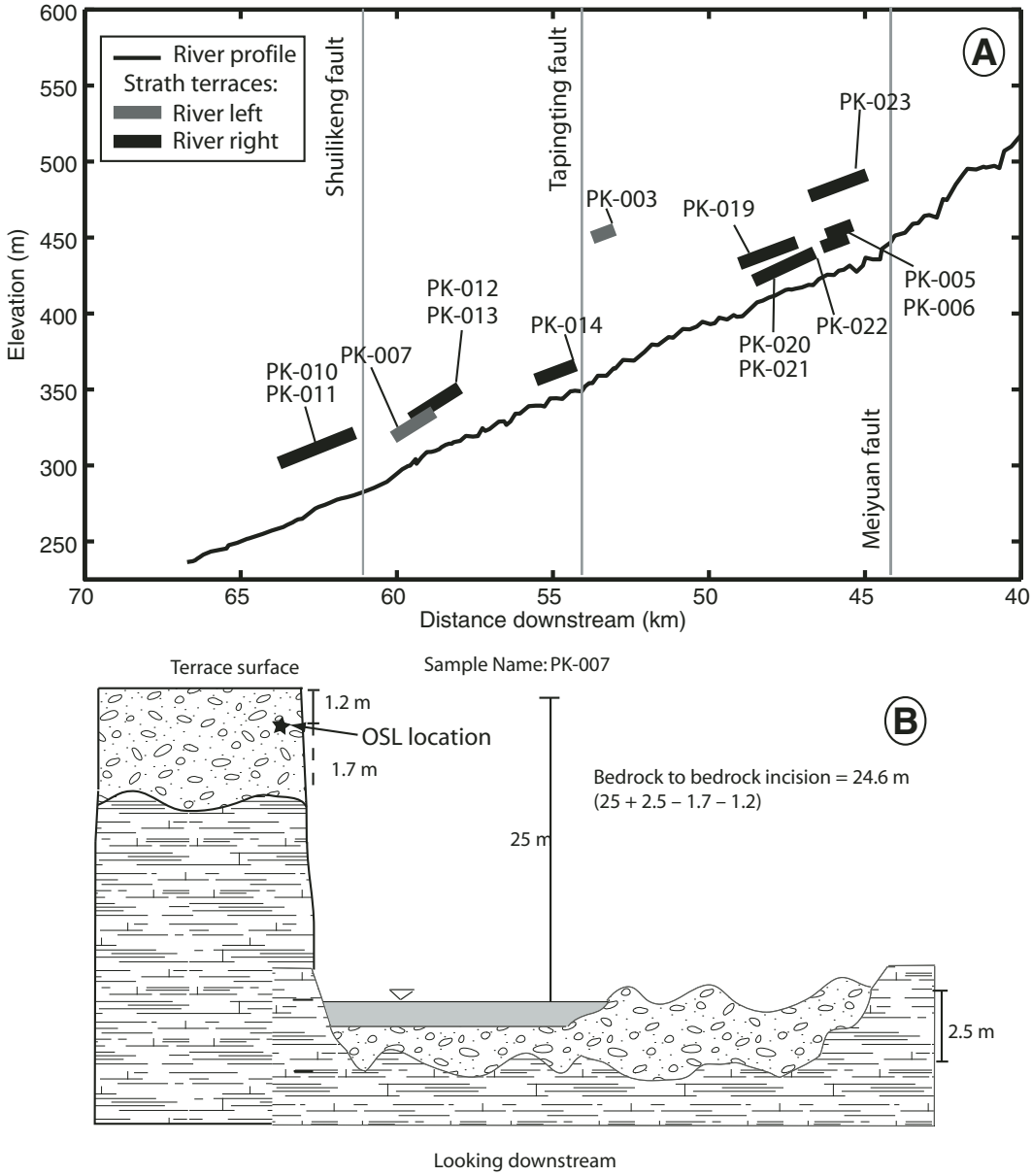

Figure 3. Schematic overview of dated strath terraces in the study area. (A) Longitudinal profile of river with schematic representation of dated terraces to show the vertical relationships between the terraces and modern river. (B) Schematic cross section of the strath terrace dated with sample PK-007. Shows how the depth of bedrock incision since the optically stimulated luminescence (OSL) date was calculated. Depth to bedrock along the river was estimated from electrical resistivity surveys along the reach (Yanites et al., 2008).

RESULTS

Channel Morphology

A regression between log-transformed slope and area yields a basinwide scaling between these parameters similar to many bedrock rivers around the world (Wobus et al., 2006) (Fig. 2A). The exponent on drainage area allows the calculation of local steepness indices, k_s, as shown in Equation 1. Values that lie above or below 370, the average for the entire basin, suggest a relatively low or high rock-uplift rate, respectively. A strong signal of high steepness index is associated with the river reaches immediately upstream of the Meiyuan and Tili faults (Fig. 2B). At the upstream end of this anomaly, k_s values increase by threefold over only a few kilometers of river length. At the downstream end, k_s values decrease by about the same amount, almost exactly coincident with the Meiyuan fault. Downstream of this high-steepness region, no clear signal exists. Although modest variations do appear to correlate with some structures, such as the Shuilikeng fault (fault D in Fig. 2B), the relatively small magnitudes make it difficult to interpret beyond inherent DEM noise and natural variability.

Channel width increases systematically with drainage area over several orders of magnitude (Fig. 5). The scaling exponent, 0.54, agrees well with other studies examining channel width (Montgomery and Gran, 2001). It should be noted, however, that significant variability exists within individual decades. In fact, regressing the data within the 10^8–10^9 m^2 drainage area decade alone gives an R^2 of just 0.09, although the scaling parameters are similar, with a coefficient of 0.0013 and an exponent of 0.56. As shown in the following, this variability of the river along a reach with similar drainage areas is an important feature of the morphological system response to active deformation. As seen in Figure 6C, the channel is narrow upstream of the Meiyuan fault (located ~45 km downstream from headwaters). Immediately downstream of the Meiyuan fault (45–50 km), the river significantly widens, reaching values of >300 m. The river narrows

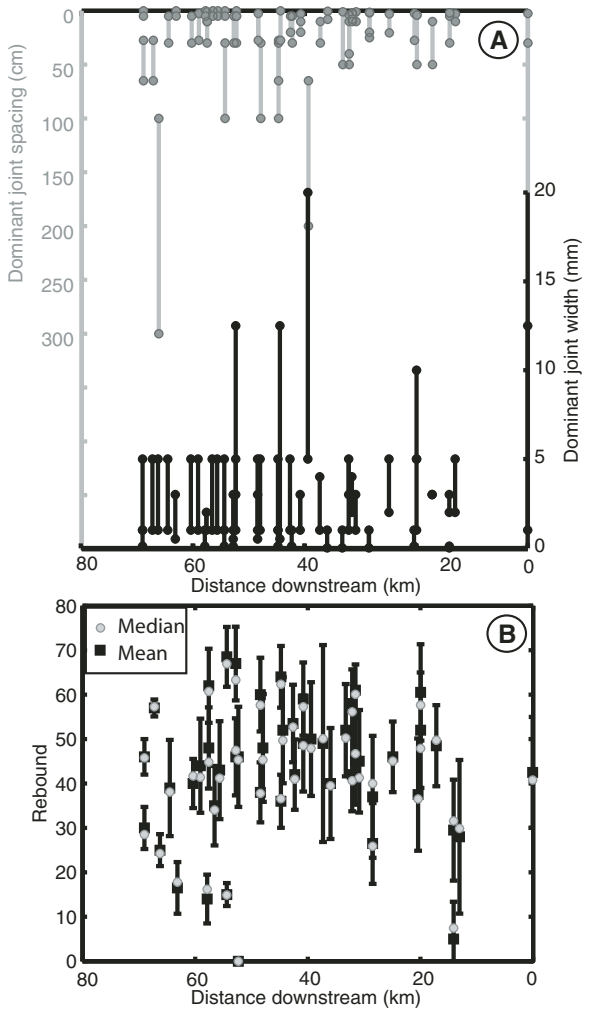

Figure 4. Results of lithology parameters. (A) Joint spacing and joint width versus distance downstream. (B) Schmidt hammer rebound values versus distance downstream. No distinct pattern in these parameters is seen along the stream path, lending support that there is no strong influence of lithology on unit stream power or shear stress estimates.

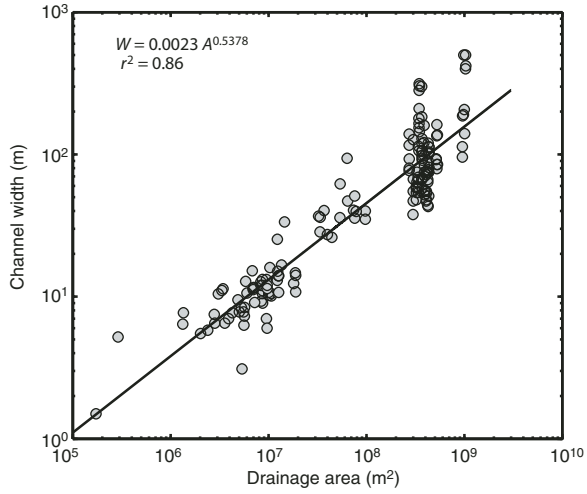

Figure 5. Log-log plot of field-measured channel width versus drainage area collected from both digital elevation model (DEM) and field analysis. The compression of data within drainage area decades 10^8–10^9 masks important variability in an area undergoing differential incision.

again over the next few kilometers. The width remains relatively constant until further narrowing occurs through the reach where the river crosses the Shuilikeng fault. Just downstream of this fault, the river widens again, and, in general, continues to do so in the downstream direction.

Unit stream power and shear stress along the Peikang River are plotted in Figures 6D–6E. Upstream of the bedrock-alluvial transition at about km 70, the stream-power and shear-stress patterns closely mimic the channel-width pattern. At the upstream end of the study reach (Fig. 6), 10 yr unit stream power and shear stress estimates from field data are extremely high (~4000 W/m^2 and ~600 Pa). Assuming a critical Shields stress of 0.05, we estimate that the shear stress is sufficient to move boulders over 0.7 m in diameter. Downstream of the Meiyuan fault, unit stream power and shear stress drop dramatically. The low values continue for a few kilometers before they begin increasing again. The unit stream power and shear stress increase over a section of about ~3–5 km. Although short-wavelength variability exists downstream of this point, unit stream power and shear stress are broadly constant to the point where the channel crosses the Shuilikeng fault. After the river passes downstream of this fault zone, unit stream power and shear stress again dramatically decline and level off as the river enters the valley immediately upstream of the Shuangtung fault. These low power and stress values continue across the Shuangtung and Chelungpu faults. The abrupt increase in unit stream power and shear stress at ~68 km is due to a large confluence where drainage area doubles through the junction, but the measured effects of channel width are subdued due to our smoothing process.

Incision Rate

The majority of our OSL samples reveal Holocene age terraces (Table 1; Table DR3 [see footnote 1]). Given the likelihood of partial resetting in these samples, we prefer the minimum age model (MAM) for terrace ages, but we also report central age model (CAM) ages as maximum ages (minimum incision rates). The MAM ages are on average 56% younger than CAM ages.

Incision rates mimic the pattern of both unit stream power and shear stress estimates (Fig. 6F). Late Quaternary to Holocene incision rates are relatively low in the 4 km downstream of the Meiyuan fault, documented by samples PK-005–PK-006 and PK-019–PK-023 (Table 1; Fig. 7). The samples suggest incision rates on the order of ~2–3 mm/yr for the last 3–12 k.y. in this reach. About 7 km downstream, incision

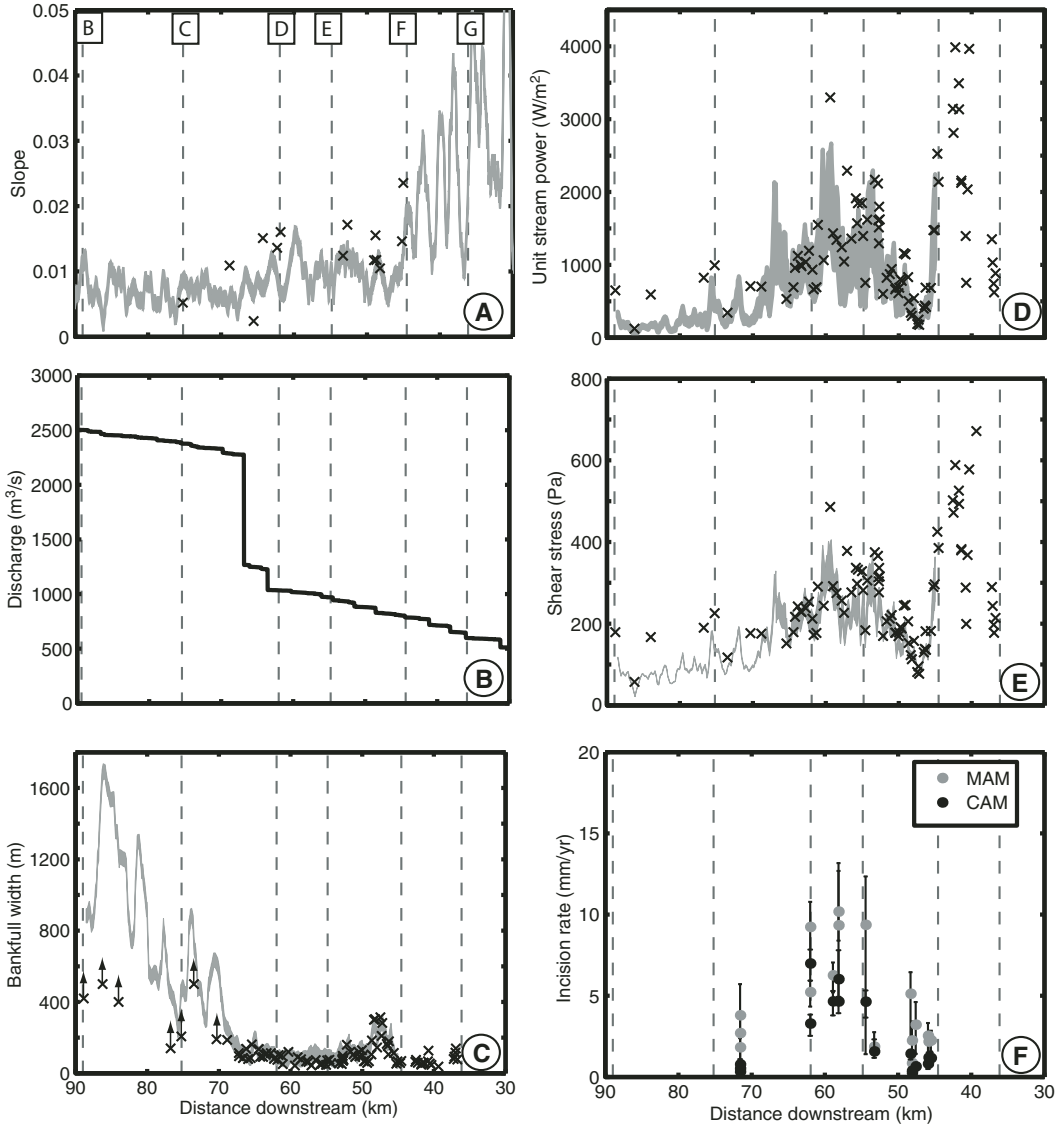

Figure 6. Channel morphology and incision rate along the river path. For A–E, digital elevation model (DEM)–derived values are denoted by gray line, the thickness of which denotes the error. Field values are the gray 'X's. (A) Channel slope. Discrepancy between field measured slope and DEM slope arises because the field data were measured only over ~100 m, whereas the DEM slope was smoothed over 1 km. (B) Contributing drainage area. (C) Channel width. The mismatch between field data and DEM measurement at the downstream end of the river was due to the horizontal limit of the laser rangefinder, which is on the order of 200–600 m, depending on the reflective surface. (D) Unit stream power. (E) Shear stress. (F) Incision rate estimates from optically stimulated luminescence (OSL) samples of sandy units on strath terraces using both minimum age models (MAM) and central age models (CAM) for interpreting the dose distributions for the samples. Dashed lines indicate, from left to right, the following structures: Chelungpu, Shuangtung, Shuilikeng, Tapingting, Meiyuan, and Tili faults.

rates increase to ~9 mm/yr and reach a maximum near the Shuilikeng fault at ~11 mm/yr. Immediately downstream of the Shuilikeng fault, a terrace capped by lateritic soil sits ~40–45 m above the river (Fig. 7). The time required for a similar lateritic soil to form in Taiwan is estimated to be around 20–30 k.y. (Tsai and Sung, 2003), suggesting a maximum incision rate of ~2 mm/yr over that time period. Further downstream, samples PK-016–PK-018 document incision rates of ~2–4 mm/yr just upstream of the Shuangtung fault. In all locations where multiple terrace levels were sampled, ages were stratigraphically appropriate (e.g., samples PK-005 and PK-006). Repeat samples ages within the same stratigraphic position are within error (PK-012–PK-013 and PK-017–PK-018).

Samples PK-030 to PK-033 were obtained from an alluvial layer blanketing an isolated strath terrace upstream of the Meiyuan fault. Unfortunately, stratigraphic inversions of the dates (samples PK-032 and PK-033 were sampled next to each other) and field evidence of recent debris-flow scour and fill on the terrace surface from small, adjacent tributaries suggest that this terrace is ill suited for OSL dating methods. The transport distance of the particles is less than a kilometer (the length of the tributary basin), and the deposits may contain reworked terrace alluvium. Both of these factors likely contribute to the unreliability of these ages. It is possible that PK-030 and PK-031 are giving the correct age and incision rates (on the order of 1–1.5 mm/yr), but based on the depositional environment and the unrepeatability of dates with samples PK-032 and PK-033, we question the robustness of the OSL dates. We report the ages in Table 1 but refrain from using them in further analysis or interpreting these data points.

Linear regression between unit stream power and incision rate results in an r^2 value of 0.58 when channel width is measured in the field or from a DEM, compared to an r^2 value of 0.05 when width is simply estimated from the traditional scaling with discharge (Fig. 8). The slope of the regression can be interpreted as an erosion susceptibility coefficient, k_ω = 0.0069 (units of mm/yr times m²/W), and the intercept represents the critical value of unit stream power, ω_c = 43.2 W/m², that must be surpassed to do work on the bedrock (Table 2). Regressions between shear stress and incision rate give very similar results, with r^2 = 0.58, k_τ = 0.046 (units mm/yr Pa), and τ_c = 65.4 Pa. We omitted sample PK-003 because it is significantly older than the other samples and thus represents a sampling of

TABLE 1. OPTICALLY STIMULATED LUMINESCENCE (OSL) AGES AND INCISION RATES

	Age (MAM; ka)	1σ	Age (CAM; ka)	1σ	Height*	+	–	Incision rate (MAM; mm/yr)	+	–	Incision rate (CAM; mm/yr)	+	–
PK003	42.11	4.25	49.84	4.19	78.50	6.60	28.40	1.86	0.51	0.89	1.58	0.40	0.74
PK005	3.26	0.81	10.20	1.93	8.30	1.10	0.90	2.54	1.29	0.78	0.81	0.32	0.22
PK006	11.66	1.90	21.18	3.45	25.40	3.60	3.40	2.18	0.79	0.57	1.20	0.44	0.31
PK007	3.93	0.55	5.28	0.81	24.60	0.10	–0.10	6.26	1.05	0.79	4.66	0.87	0.64
PK010	6.61	0.78	10.48	1.69	34.50	1.10	0.90	5.22	0.89	0.70	3.29	0.76	0.55
PK011	3.78	0.61	4.99	0.52	34.90	1.10	0.90	9.24	2.14	1.54	6.99	1.05	0.86
PK012	3.00	0.74	6.03	0.79	28.00	0.10	5.40	9.34	3.10	3.35	4.65	0.72	1.36
PK013	2.90	0.42	4.90	0.74	29.50	0.10	5.40	10.18	1.79	2.99	6.02	1.09	1.78
PK014	1.35	0.61	2.72	0.46	12.60	0.10	–0.10	9.36	7.96	2.98	4.63	0.98	0.70
PK016	5.36	1.27	30.35	7.08	9.80	5.80	1.20	1.83	1.99	0.56	0.32	0.35	0.10
PK017	2.13	1.06	15.32	4.02	8.10	1.10	1.90	3.80	4.77	1.92	0.53	0.29	0.22
PK018	3.07	0.92	10.62	2.69	8.30	1.10	1.90	2.70	1.67	1.15	0.78	0.40	0.32
PK019	4.66	1.59	16.70	3.24	23.90	0.10	–0.10	5.13	2.69	1.32	1.43	0.35	0.24
PK020	8.18	2.03	27.67	5.35	7.00	0.10	1.90	0.86	0.30	0.38	0.25	0.07	0.10
PK021	3.12	1.45	18.14	4.36	7.00	0.10	1.90	2.25	2.02	1.17	0.39	0.13	0.17
PK022	2.79	0.98	13.87	2.66	9.00	0.10	1.90	3.22	1.80	1.39	0.65	0.16	0.23
PK023	9.10	1.07	17.56	3.07	20.50	3.10	3.40	2.25	0.69	0.59	1.17	0.46	0.35
PK030	3.45	0.46	6.18	0.38	5.4	0.1	0.1	1.56	0.03	0.03	0.87	0.016	0.016
PK031	13.79	1.06	26.8	1.87	42.2	4	4	3.06	0.29	0.29	1.57	0.15	0.15
PK032	2.09	0.55	6.56	0.63	6	5	1	2.87	2.39	0.48	0.91	0.76	0.15
PK033	10.04	1.26	20.5	1.49	6	5	1	0.60	0.50	0.10	0.29	0.24	0.049

Note: The + refers to the minimum thickness of alluvium between the bedrock surface and the observed alluvium, i.e., the observed thickness of alluvium between the OSL sample location and the bottom of the outcrop. If bedrock is exposed, this value is the measurement error of the laser rangefinder that was used to estimate height above the modern river. The – refers to the maximum alluvium estimated by the first appearance of bedrock found below the outcrop of OSL sample.
*Height refers to the best estimate of bedrock-to-bedrock incision depth.

a much broader time period and potentially different climate; however, inclusion of this sample in the regressions does not significantly change the outcome.

Visual and statistical inspection of estimated rock strength (Table DR4 [see footnote 1]) and its relationship with unit stream power and shear stress reveals no significant variation in erosion susceptibility along the study reach except for downstream of the Shuangtung fault, where Schmidt hammer rebound values were consistently zero (Fig. 4). Regression between Schmidt hammer rebound and either unit stream power or shear stress results in r^2 values of 0.034 and 0.032, respectively.

DISCUSSION

Calibrated River Incision Rule

Unit stream power and shear stress are robust proxies for incision rate in the Hsuehshan Range in central Taiwan (Fig. 8). Unit stream power and shear stress are strongly controlled by reach-scale variations in channel width that deviate from estimates of width based on drainage area. It is interesting, however, that upstream of the Meiyuan fault, strong changes in steepness index suggest that slope is an important morphological parameter for part of the landscape. We note that the steepness indices are variable in this reach. One possibility is that the variability results from propagating knickpoints set off by earthquakes on the Meiyuan fault. This is certainly a possibility; however, we do not observe any preserved knickpoints in the field. Instead, this variability is probably a result of the channel and valley width approaching the pixel resolution of the DEM (20 m). This causes particularly narrow zones to be elevated on the DEM with respect to the real riverbed elevation because the pixel value includes significant parts of the hillslopes. It is clear that the average of the steepness indices is still significantly higher than downstream. Field observations indicate that channel width, although variable, tends to be very narrow compared to upstream reaches in this section of river, further enhancing unit stream power and shear stress. One question that is difficult to address with these data is: does the rate of river incision match the vertical rock-uplift rate relative to the geoid? If we assume that it does, then channel dynamics can be used to map tectonic deformation in the Taiwan orogen. The correlative changes in unit stream power, shear stress, and incision rate, associated with mapped structures, are consistent with the hypothesis that the river morphology has indeed adjusted to match rock uplift. Given the high rates and variability

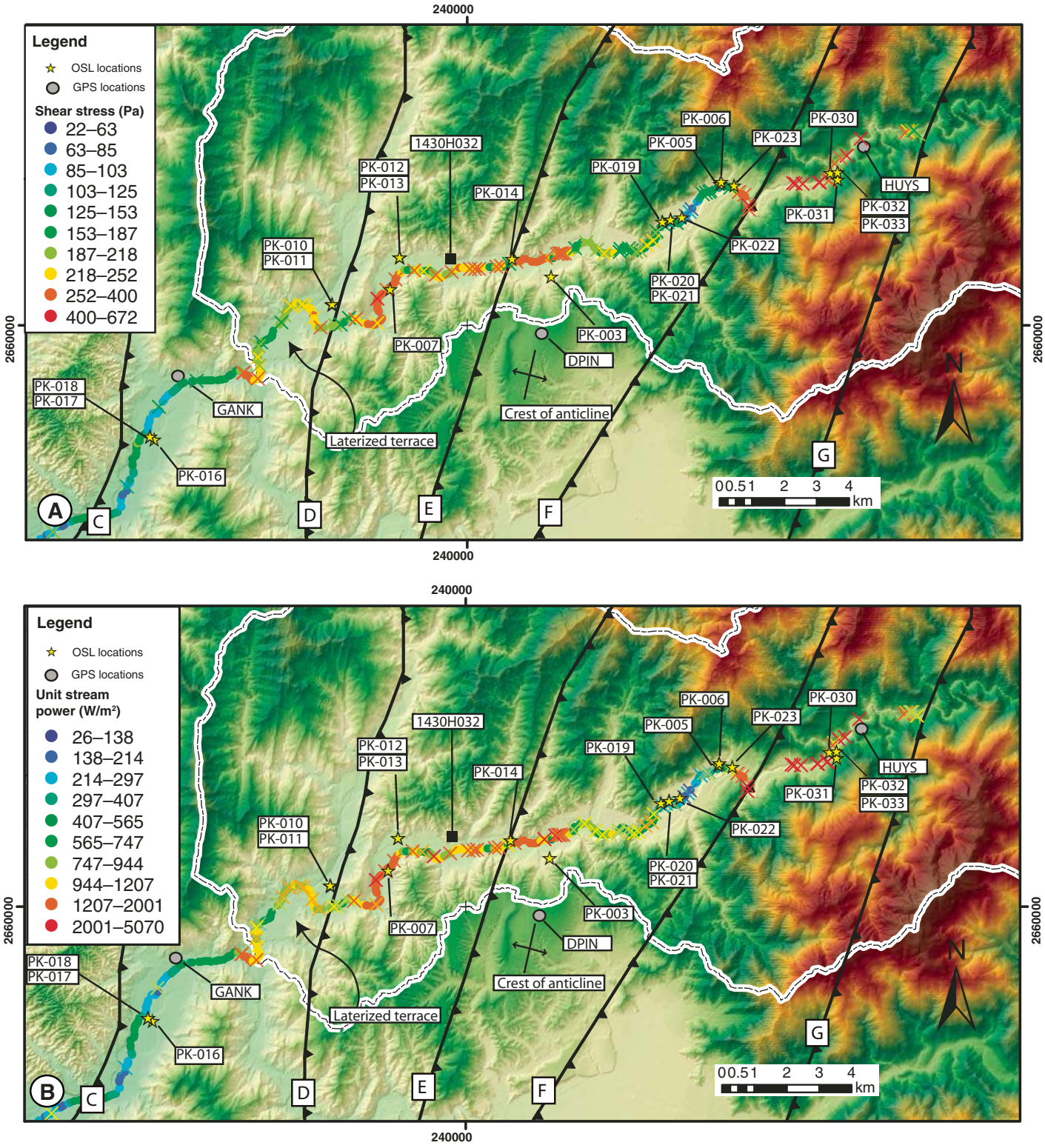

Figure 7. Shear stress (A) and unit stream power (B) values in map space. Circles are digital elevation model (DEM) data; 'X's are field data. Stars are locations of optically stimulated luminescence (OSL) samples, and gray circles are the locations of the three global positioning system (GPS) stations along the river path. Black box denotes the local river gauging station. Faults are labeled C–G (from Fig. 1B), representing, from left to right, the following structures: Shuangtung, Shuilikeng, Tapingting, Meiyuan, and Tili faults.

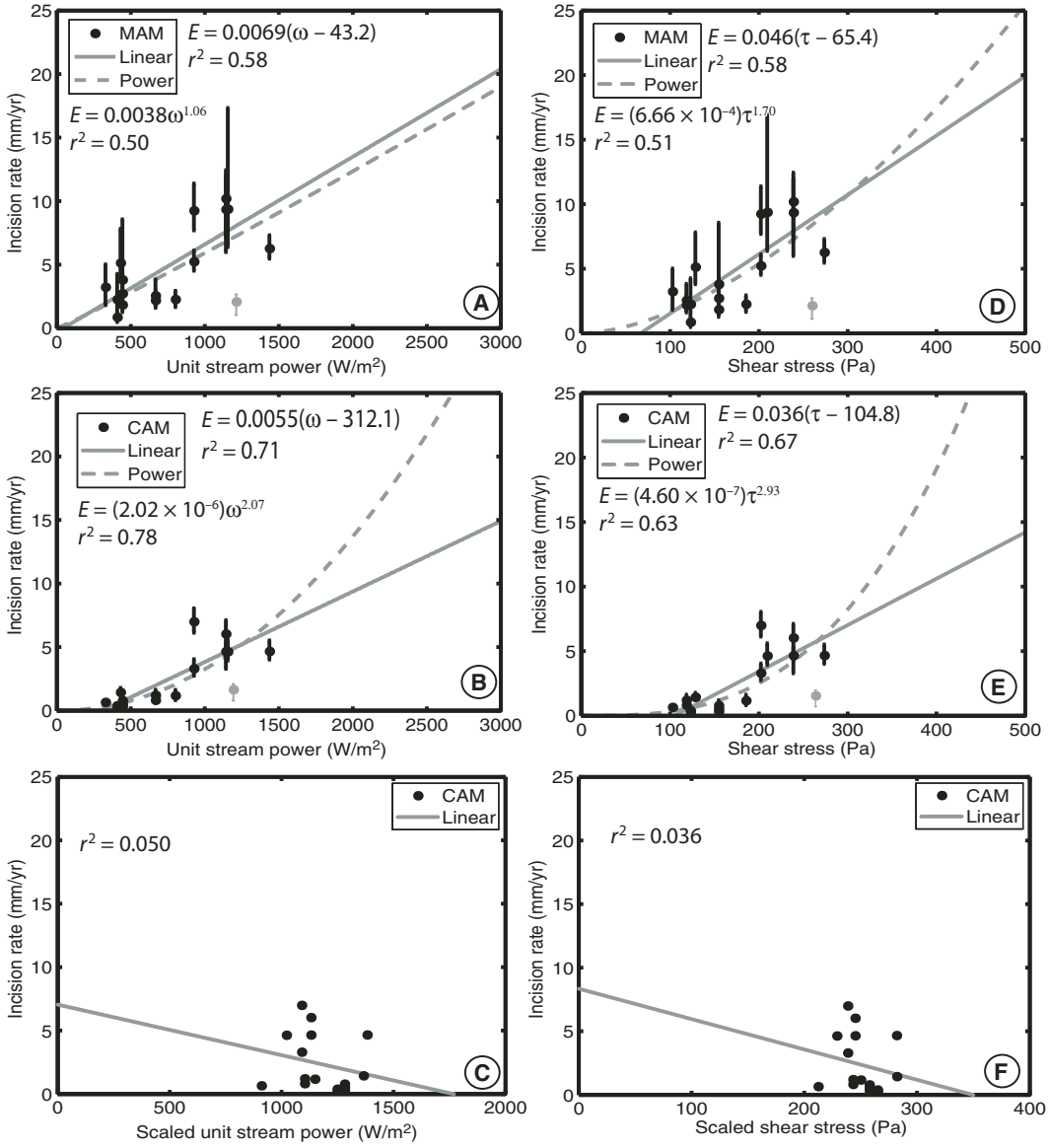

Figure 8. Calibrated river incision rules. Linear and power-law regressions were performed on unit stream power (A and B) and shear stress (D and E), and incision rates were estimated from both minimum age models (MAM) (A and D) and central age models (CAM) (B and E) ages. (C and F) Linear regressions between unit stream power/shear stress and CAM incision rates using scaled channel width values rather than measured values as has been done in the past. The regression values are used to estimate incision rate upstream of the Meiyuan fault. Use of MAM incision rates does not change the regression significantly. Sample PK-003 is plotted in gray but was not included in the regression analyses because it is significantly older than all other samples.

of erosion, if erosion rates did not match rock-uplift rates, it would not take long to produce slopes greater that what is observed. For example, a 4 mm/yr erosion difference over a distance of 10 km would generate a 40% slope, if it were sustained for 1 m.y.; actual slopes along the study reach are on the order of 1%–2%. Further, qualitative analysis of hillslope and gross drainage basin morphology suggests a similar trend to the pattern of incision and unit stream power and shear stress (Fig. 9). Areas with the steepest slopes and highest local relief generally coincide with the most powerful river reaches, and vice versa. This indicates that the spatial variations in Holocene incision rate have been sustained for long enough to be reflected in the regional topography. We do not know what this time scale is, but a reasonable guess is that it is comparable to the ratio of hillslope relief (order hundreds of meters) to erosion rate (order millimeters per year), or roughly 10^5 yr.

TABLE 2. REGRESSION RESULTS

		MAM			CAM		
		p_1	p_2	R^2	p_1	p_2	R^2
Unit stream power	Linear	0.0069	43.2	0.58	0.0055	312.1	0.71
	Power	1.06	.0038	0.50	2.07	2×10^{-6}	0.78
Shear	Linear	0.046	65.4	0.58	0.036	104.8	0.67
	Power	1.70	6.7×10^{-4}	0.51	2.93	4.6×10^{-7}	0.63

Note: In the linear model, p_1 is the slope and p_2 is the intercept. In the power-law model, p_1 is the exponent and p_2 is the coefficient.

A steady-state bedrock river results in a longitudinal profile that does not change with time because any differential vertical motion along the river's path is matched by corresponding differential vertical incision. To date, the most common model of channel dynamics in a tectonically active region uses an approximation of river dynamics, where drainage area, *A*, is used in place of both discharge and channel width, to explore steady-state and transient river morphology. Because this approach scales

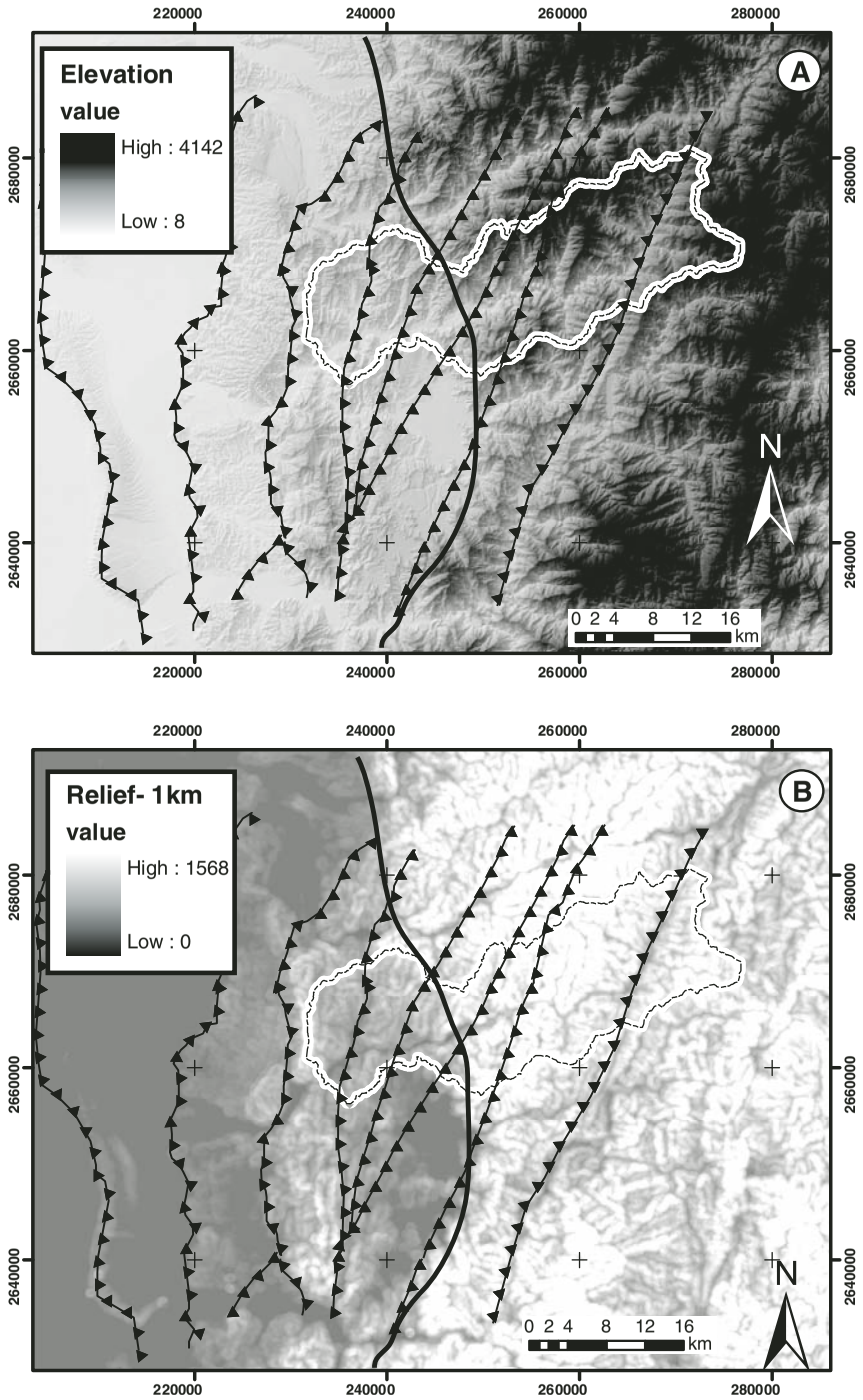

Figure 9. Hillslope morphology around the Puli Basin region. (A) Hillshade draped with 20 m digital elevation model. (C) Relief within a 1 km radius of each pixel. (B) Slope calculated in 3 × 3 pixel windows. Peikang Basin is outlined with dotted line. Black in A and B, and white line in C are location of physiographic transition denoted in Figure 2. Fault locations are taken from Powell (2003) and are only plotted to the extent of her field area.

the cross-sectional geometry with contributing drainage area, a change in channel bed elevation, and thus slope, is the only morphological parameter that is able to adjust the local channel hydraulics and therefore change the incision rate to match rock-uplift rate. However, several recent studies have highlighted the importance of channel width as an additional control on (as well as a product of) the rate of channel incision into bedrock (Duval et al., 2004; Finnegan et al., 2005; Whittaker et al., 2007; Wobus et al., 2008). Along some rivers, including the Peikang, slope and drainage area alone do not provide a sufficient proxy for stream power or shear stress because both quantities are strongly influenced by downstream variations in channel width.

To use channel morphology as a tool to map changes in rates of rock uplift, it is necessary to understand the feedbacks between morphology (chiefly width and slope) and other potential influences (such as sediment cover and sediment supply). It is quite possible, and in fact likely, that the dynamics of the processes that widen a channel are different from those that lower the channel thalweg. Further, it is likely that the time scale for adjustment in width is generally much shorter than the time scale for gradient adjustment. Based on the modeling work of Wobus et al. (2006b), we conjecture that width adjustment could occur over a time scale related to the water depth divided by incision rate. Establishing the controls on this time scale, and more generally unraveling the environmental controls on channel dynamics and morphology, will require carefully mapping of channel geometry in regions undergoing differential incision.

Assuming the Peikang River is in steady state with the rock-uplift rate, we can calibrate a fluvial incision rule based on estimates of unit stream power or shear stress. Using the regression coefficients (Fig. 8; Table 2), we can calculate both an "erodibility" factor (k_ω and k_τ) and a threshold term (ω_c and τ_c) for Equations 2 and 3. It is of particular note that this calibration does not work if one simply scales channel width with drainage area. It is interesting to compare the estimated threshold values with motion thresholds associated with bed material in the Peikang. Using a critical Shields stress of 0.05 and a grain density of 2700 kg/m^3, the threshold shear stress estimated from the regression in Figure 8 corresponds to a median bed grain size of 7.7 cm. The equivalent for ω_c (using $\omega_c = \tau_c U_{*c} = \tau_c^{3/2}/\rho$, where ρ is water density) is 14.4 cm. By comparison, point counts of grain size at 45 locations along the Peikang reveal a median grain size of ranging from ~5 to ~30 cm, with a mean of around ~15 cm, i.e., well within the expected range given ω_c and τ_c, suggesting that these values are indeed set by the caliber of sediment fed to the river system. In a subsequent section on tectonic implications, we use the calibrated river incision rule to estimate differential rates of rock uplift in places where we do not have strong control on incision rate.

Implications for a Minimum Channel Width

The major morphological adjustment of the river reach to enhanced rock uplift just upstream of the Shuilikeng fault is channel narrowing. Upstream of the Meiyuan and Tili faults, however, the morphological adjustment to enhanced rock uplift is both channel narrowing and steepening. One explanation for the different morphological adjustments between these areas calls upon the distribution of energy dissipation and shear stress in a bedrock channel. As implied by our calibrated incision rule, the unit stream power and shear stress proxies assume that erosion is primarily vertical. As a channel narrows while it erodes in response to downstream tilting or passage of a fault-generated knickpoint, the channel walls will account for a higher proportion of its wetted perimeter. If a channel becomes too narrow, then a significant proportion of boundary stress and energy dissipation occurs on the channel walls, reducing the efficiency of the channel's vertical erosive potential (Wobus et al., 2008). Further narrowing will not increase vertical incision on the channel bed. At this point, the only parameter able to adjust to increase the erosive potential of the stream is the slope, and a knick zone will develop in response to further enhanced rock uplift.

If this conceptual model is correct, then temporal changes in channel width must occur faster than changes in slope. We propose two general time scales of dynamic channel adjustment to a perturbation in central Taiwan. We take the vertical drop between thrust faults as the appropriate length scale that needs to be adjusted to change channel slope in response to a change in rock-uplift rate. Between the Meiyuan and Shuilikeng faults, the vertical drop is ~100 m (slope of 1% over a distance of 10 km). A rock-uplift rate of 10 mm/yr gives a time scale of ~10 k.y. for the adjustment of channel slope upstream of the Shuilikeng fault. Alternatively, we postulate that channel width can adjust over the time needed to vertically erode through one channel depth. Estimates of floodwater depth in this reach are on the order of 10 m. A 10 mm/yr incision rate gives a time scale of only ~1 k.y. to adjust channel width. Using these time scales as a guide, we posit that rivers in this region will first narrow in response to enhanced rock uplift. If it can narrow enough to increase unit stream power and shear stress to a level that will bring the incision rate into balance with the relative rock-uplift rate, then no slope adjustment will take place; however, if the channel narrows to the point where boundary friction and energy dissipation on the walls become significant, then the vertical adjustment of channel slope will occur, producing a zone of high steepness indices.

We calculated the width-to-depth ratio of the channel as a test of this hypothesis (Fig. 10). Wobus et al. (2008) suggested that a width-to-depth ratio on the order of 5–10 represents the point at which wall effects become important. We find a minimum width-to-depth ratio of around 12 for both the reach upstream of the Meiyuan fault (F in Fig. 10) and for the reach just upstream of the Shuilikeng fault (D in Fig. 10). Our estimated incision rate upstream of the Meiyuan and Tili faults is higher than at the apex of the Shuilikeng fault. We suggest that the reaches upstream of the Meiyuan and Tili faults reached their minimum width but were unable to match the rock-uplift rate; therefore, a strong slope signal has developed to further

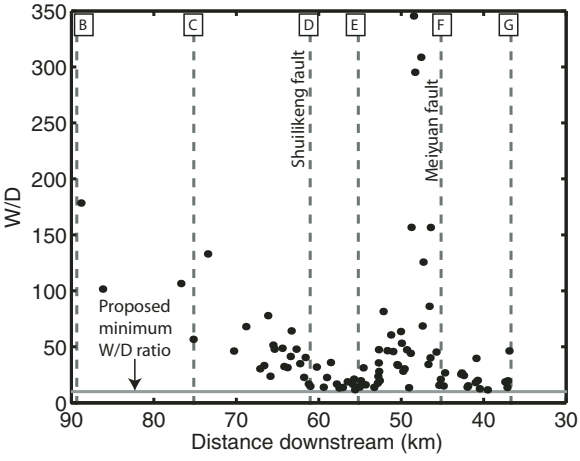

Figure 10. Width-to-depth ratio (W/D) as a function of distance downstream. The lowest values correlate with locations where we have either measured or inferred enhanced rates of river incision. Notice no values exist below a W/D of 10, denoted by gray line. We propose that when W/D ratios are <10, the only mechanism to increase unit stream power and/or shear stress is channel steepening.

enhance unit stream power and shear stress. A very minor steep reach (k_s ~ 500, compared to the average of 370) in the ~1 km upstream of the Shuilikeng fault suggests that this stretch of river has narrowed to the minimum width but remains near the threshold to develop a knick zone, or zone of relative channel steepening compared to the contributing drainage area.

The essence of our hypothesis for bedrock channel response is as follows. First, provided that the width-to-depth ratio is sufficiently large (Fig. 10, just downstream of the Meiyuan fault), any steeping due to relative base-level fall along the river (for example, tilting above a fold limb or creation of a fault scarp across the channel) will increase the speed of the current and thereby decrease both the width and the cross-sectional area of the channel. All else being equal, this narrowing will tend to produce a higher rate of incision (e.g., as the river approached the Shuilikeng fault), until a balance is reached between the incision rate and the local rate of rock uplift relative to a base-level datum downstream (such as a coastline). Indeed, this mechanism has been reproduced in numerical models of channel cross-section hydraulics and erosion (Stark, 2006; Turowski et al., 2007; Wobus et al., 2006b). However, if the width-to-depth ratio becomes smaller than a critical value, further narrowing will tend to be counteracted by an increase in stress and erosion along the walls, and will therefore tend not to increase vertical incision rates. Consider a bedrock channel above an active fold limb that has achieved a width-to-depth ratio that maximizes stress. If the incision rate is lower than the rate of fold-limb growth, the channel will continue to steepen (but not widen) until the incision rate balances the rate of fold growth. In other words, according to this hypothesis, a wide channel is expected to respond to differential rock uplift with a combination of steepening and narrowing, while a narrow channel will only steepen (e.g., upstream of the Meiyuan fault; Fig. 10). This hypothesis suggests that both the reaches upstream of the Shuilikeng and the Meiyuan/Tili faults have reached the minimum width in response to enhanced rock-uplift rate; however, the much greater rock-uplift rates upstream of the Meiyuan and Tili faults have further caused the development of a knick zone, whereas the reach upstream of the Shuilikeng fault can accomplish almost all of the work by simply narrowing.

Tectonic Implications

It is clear that changes in channel morphology and incision rate along the Peikang River in central Taiwan are associated with faults and/or folds. To the extent that these patterns reflect differential rock motion, they reveal important information on the strain budget for the orogen upstream of the Shuangtung fault (Fig. 11). In our field study, two distinct stretches of river appear to have similar lithologies but show distinctly different geomorphic signals. The boundary between these two reaches appears to be the Meiyuan fault. We hypothesize that this boundary represents an important geologic structure within this part of the Hsuehshan Range, which we discuss in the following.

Upstream of the Meiyuan Fault

Using our calibrated incision model (Fig. 8), we can estimate the incision rate along this reach from the linear unit stream power and shear stress models. Assuming the 10 yr mean unit stream power is around 2000 W/m^2 and shear stress is 350 Pa (Fig. 6), the minimum incision rate using the linear CAM models is ~9 mm/yr. The maximum rate from linear MAM models is ~13.5 mm/yr. Our estimated incision rates are significantly higher than previously proposed, e.g., ~1–6 mm/yr from thermochronological and suspended sediment data (Dadson et al., 2003; Simoes et al., 2007a). One way to reconcile these estimates is to consider that our calibrated model is only valid over the Holocene and that discharge might have been lower during glacial periods. Another study has found a late Holocene increase in incision rate for the Ehrjen River basin in southern Taiwan (Hsieh and Knuepfer, 2001). Another possibility is the observed variability in thrust activity in analog and numerical models of critical wedges, which suggest short-term enhanced rates of rock uplift that "jump" around the orogen as thrusts turn on and off to maintain taper (Hoth et al., 2006; Naylor and Sinclair, 2007; Upton et al., 2009). Despite the potential temporal variability in incision rate, this area is clearly incising faster than elsewhere along the flow path. The strong change in hillslope morphology (Fig. 9) suggests that this erosion is long-live, and thus, this area is likely experiencing a significantly higher rate of rock uplift than the foothills to the west and possibly the Central Range to the east.

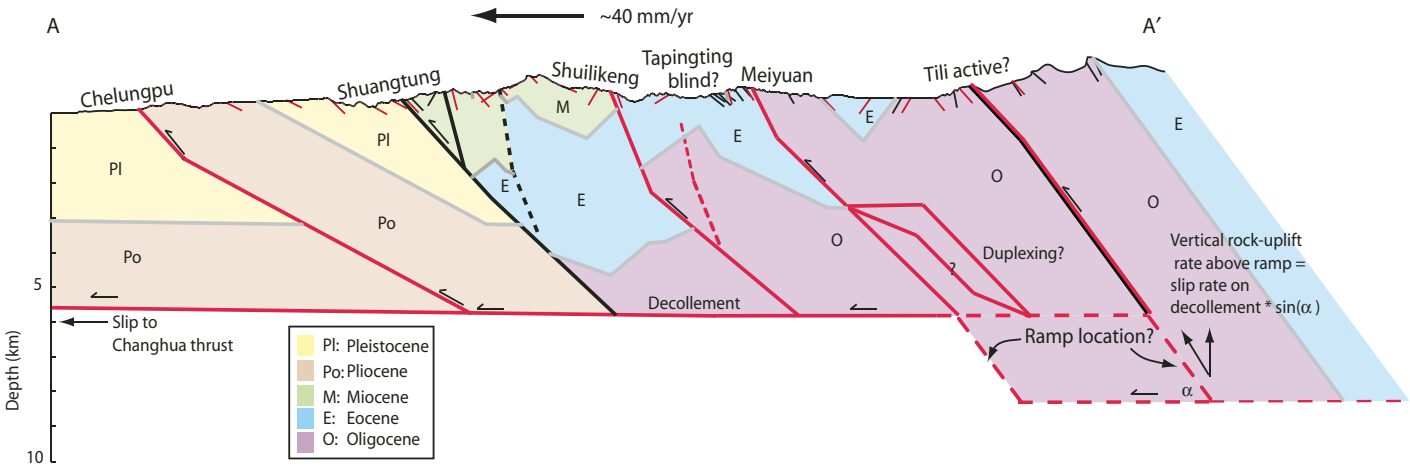

Figure 11. Schematic cross section through the field area. Location is shown in Figure 1. Red faults highlight actively deforming structures. The Chelungpu was the location of the 1999 Chi-Chi earthquake. The other interpreted active faults result from our channel morphology and incision rate study. The exact cause of the high rates of rock uplift upstream of the Meiyuan and Tili faults is unknown, but we include diagrammatic sketches of a ramp in the décollement, which is required to bring up deeper structural levels in the orogen, and duplexing, both of which could potentially drive these high rates.

Previous work on the structural (Yue et al., 2005) and tectonic framework (Fuller et al., 2006; Simoes et al., 2007a) of this area suggests that there is likely to be a zone of enhanced rock uplift that coincides roughly with the reach upstream of the Meiyuan and Tili faults. Based on structural reconstructions, a stepping-down of the décollement is required to bring the older rocks of the Hsuehshan Range up to the surface (Powell, 2003). Yue et al. (2005) proposed that the location of this ramp is below the Tili fault; however, the exact location and dip of this ramp are poorly constrained (Fig. 11). This structural solution implies that any slip along a steeply dipping décollement will result in a zone of higher rock-uplift rate (relative to the footwall) above it. Assuming that the décollement is slipping at ~35 mm/yr (Yue et al., 2005), then our calibrated incision rates imply a ramp dip of ~15°–23° (calculated with the equation dip = $\sin^{-1}$[incision rate/décollement slip rate]). Alternatively, this region has been proposed to be a focus of tectonic underplating via duplexing (Fig. 11) as material is transported vertically from the subducting plate of the continental margin into the overlying wedge (Fuller et al., 2006; Simoes and Avouac, 2006). This is supported by relatively young mineral cooling ages just to the north of the Peikang River and east of the Meiyuan fault (Fuller et al., 2006; Liu et al., 2001; Simoes et al., 2007a). Simoes et al. (2007a) suggested that the underlying rocks are likely to be quite hot, and the exhumation rate in this area is likely to be relatively high. Thus, based on the various structural and tectonic frameworks proposed by others (Fuller et al., 2006; Simoes et al., 2007a; Yue et al., 2005), the region upstream of the Meiyuan fault consistently stands out as a location of rapid and sustained rock uplift. Our results support this assertion, although we cannot distinguish between a long-lived thrust ramp or underplating by duplexes.

River Reach between the Meiyuan and Shuangtung Faults

The segment that lies in the ~4-km-long stretch immediately downstream of the Meiyuan fault is a zone of relatively low unit stream power, shear stress, and incision rate (Table 1; Fig. 7). Observations of regional structure, morphology, and ground motion associated with the Chi-Chi earthquake may help to interpret the significance of this low-incision zone, although a definitive answer remains elusive. First, other rivers in this region, such as the Tachia and Cho Rivers, have similarly wide reaches immediately downstream of the physiographic transition denoted by the gray line in Figure 9. This physiographic transition is highlighted by greater local relief and hillslope gradients to the east of this line. Another potentially important observation is that a continuous GPS station at the south end of the Puli Basin (almost due south of this reach) recorded downward motion during the 1999 Chi-Chi earthquake (Yue et al., 2005). If that coseismic motion is not fully recoverable, this could explain the lower incision rates (i.e., rock-uplift rates) in this segment, since the downstream end of the river would experience reduced base-level lowering due to this gradient in rock uplift. Finally, if the Meiyuan fault marks the location of the main décollement stepping down to deeper structural levels (Fig. 11), then this segment could correlate with the location where the décollement flattens at higher levels to the west (i.e., the top of the ramp in the décollement), causing a distinct decrease in the local rock-uplift rate relative to upstream.

The downstream increase and then abrupt decrease in incision rate, unit stream power, and shear stress across the Shuilikeng fault suggest that, at least over the Holocene, the fault is active (Fig. 11). Slip occurs along an east-to-west steepening thrust ramp that either offsets the ground surface or terminates within a broader sheared forelimb of a fault-propagation fold. Active shortening at the surface this far into the interior of a critical wedge is unusual, but not necessarily surprising. Backstepping of the deforming wedge can occur in cases of mass imbalance, and in this case, is most likely related to rapid erosion in the Puli region (Powell, 2003; Upton et al., 2009). Evidence for active slip on the Shuilikeng fault was also suggested by Sung et al. (2000), who compared leveling surveys done in 1904 and 1985 and found statistically significant changes in channel slope immediately upstream of the Chelungpu and Shuilikeng faults. They interpreted this small change in steepness as indicating that these faults are active, although the change in slope was only ~10% of the actual slope and did not account for survey and co-registration errors. Finally, deformation of late Pleistocene alluvium in the Puli Basin is also consistent with an active Shuilikeng fault (Powell, 2003).

Deformed terraces in the Puli Basin to the south support our assertion for active strain, as defined by geomorphic analysis, in the Peikang River valley. Figure 7 highlights an anticlinal axial surface that appears to correlate with a small spike in unit stream power and shear stress in the Peikang River. A syncline is mapped to the west (Powell, 2003) and appears to correlate with a small drop in unit stream power and shear stress. The coincidence between mapped axial surfaces in folds that deform synorogenic and older strata in the Puli Basin and the relative magnitude of fluvial erosion potential in the Peikang River lend further supports to our assessment that the incision rate, rock-uplift rate, and channel morphology are in a state of equilibrium. Dates on these fill terraces give ages of ca. 50 ka (Powell, 2003). Unfortunately the Pleistocene sediments are not preserved across the Shuilikeng fault and thus cannot be used to constrain the long-term strain there.

Comparison with Geodetic Data

Since the 1999 Chi-Chi earthquake, the number of GPS stations monitoring displacement has grown. Three stations can be found along the Peikang River (Fig. 7). Using publicly available rates (http://gps.earth.sinica.edu.tw), we derived the vertical displacement for these stations using a station (CIME) on the Penghu Islands west of Taiwan as the reference station. The station GANK is located in the valley immediately upstream of the Shuangtung fault and ~1.5 km upstream of OSL samples PK-016, –017, and –018. The station has recorded a vertical velocity of 1.3 ± 0.3 mm/yr between 2000 and 2006, as compared to our incision rate estimate of ~2–4 mm/yr. Station DPIN sits on a large folded terrace at the north end of the Puli Basin, just 2 km south of the Peikang River. It lies at the upstream end of the enhanced stream-power zone associated with the Shuilikeng fault. A vertical velocity of 5.8 ± 0.2 mm/yr between the years of 2002 and 2008 was recorded. This station lies close to the transition between the low-incision zone downstream of the Meiyuan fault (~1–2 mm/yr) and the enhanced incision zone upstream of the Shuilikeng fault (~10 mm/yr). Finally, a station between the Meiyuan and Tili faults in the Hsuisan Forest was established in 2006. Since then, this station, HUYS, has recorded a vertical velocity of 7.6 ± 0.4 mm/yr, which is slightly below our lower bound estimate of 9 mm/yr. Thus, the GPS-derived vertical velocity pattern is broadly consistent with the terrace-derived incision-rate pattern. Although the time scales of these comparisons differ by about three orders of magnitude, we feel that the similar patterns are further support to our assertion that incision is keeping pace with rock-uplift rate relative to the geoid.

CONCLUSIONS

Channel morphology and dynamics are ideal tools for mapping differential rock uplift in the Taiwanese orogen, if carefully employed. As may be the case for many landscapes, it is important to consider variation in channel width along with channel slope to properly calibrate and apply a river incision rule for a region. Two separate stretches of the Peikang River in central Taiwan respond to locally enhanced rock-uplift rates with different morphological signals.

Upstream of the Meiyuan fault, the river is both steep and narrow compared to its drainage area. Given the calibrated river incision rule, we estimate the stream incision rate in this reach to have been ~9–13.5 mm/yr over the Holocene. Downstream of the Meiyuan fault, an increase in incision rate, unit stream power, and shear stress across the Shuilikeng fault suggests it is currently active. Incision rate across this reach increases to ~10 mm/yr from a minimum of ~1 mm/yr. Finally, evidence from the Peikang River supports a model of river response in which a river will narrow to increase its erosive potential until a minimum width is reached, and only after this occurs will the river's slope increase and develop a persistent knick zone.

ACKNOWLEDGMENTS

Funding was provided by National Science Foundation grant EAR-0510971 and a National Defense Science and Engineering Graduate Fellowship to Yanites. The manuscript benefited from thorough reviews from Mark Quigley, associate editor John Fletcher, and an anonymous reviewer.

REFERENCES CITED

Arnold, L.J., Balley, R.M., and Tucker, G.E., 2007, Statistical treatment of fluvial dose distributions from southern Colorado arroyo deposits: Quaternary Geochronology, v. 2, no. 1–4, p. 162–167, doi: 10.1016/j.quageo.2006.05.003.

Chen, W.S., Lee, K.J., Lee, L.S., Ponti, D.J., Prentice, C., Chen, Y.G., Chang, H.C., and Lee, Y.H., 2004, Paleoseismology of the Chelungpu fault during the past 1900 years: Quaternary International, v. 115, p. 167–176, doi: 10.1016/S1040-6182(03)00105-8.

Chen, Y.G., Lai, K.Y., Lee, Y.H., Suppe, J., Chen, W.S., Lin, Y.N.N., Wang, Y., Hung, J.H., and Kuo, Y.T., 2007, Coseismic fold scarps and their kinematic behavior in the 1999 Chi-Chi earthquake Taiwan: Journal of Geophysical Research–Solid Earth, v. 112, no. B3, p. 1–15.

Dadson, S.J., Hovius, N., Chen, H.G., Dade, W.B., Hsieh, M.L., Willett, S.D., Hu, J.C., Horng, M.J., Chen, M.C., Stark, C.P., Lague, D., and Lin, J.C., 2003, Links between erosion, runoff variability and seismicity in the Taiwan orogen: Nature, v. 426, no. 6967, p. 648–651, doi: 10.1038/nature02150.

Dahlen, F.A., and Barr, T.D., 1989, Brittle frictional mountain building: 1. Deformation and mechanical energy budget: Journal of Geophysical Research–Solid Earth and Planets, v. 94, no. B4, p. 3906–3922, doi: 10.1029/JB094iB04p03906.

Dahlen, F.A., and Suppe, J., 1988, Mechanics, growth, and erosion of mountain belts *in* Clark, S.P., Burchfiel, B.C., and Suppe, J., eds., Processes in Continental Lithospheric Deformation: Geological Society of America Special Paper 218, p. 161–178.

Duval, A., Kirby, E., and Burbank, D., 2004, Tectonic and lithologic controls on bedrock channel profiles and processes in coastal California: Journal of Geophysical Research–Earth Surface, v. 109, no. F3, p. 1–18.

Finnegan, N.J., Roe, G., Montgomery, D.R., and Hallet, B., 2005, Controls on the channel width of rivers: Implications for modeling fluvial incision of bedrock: Geology, v. 33, no. 3, p. 229–232, doi: 10.1130/G21171.1.

Flint, J.J., 1974, Stream gradient as a function of order, magnitude, and discharge: Water Resources Research, v. 10, no. 5, p. 969–973, doi: 10.1029/WR010i005p00969.

Fuller, C.W., Willett, S.D., Fisher, D., and Lu, C.Y., 2006, A thermomechanical wedge model of Taiwan constrained by fission-track thermochronometry: Tectonophysics, v. 425, no. 1–4, p. 1–24, doi: 10.1016/j.tecto.2006.05.018.

Galbraith, R.F., Roberts, R.G., Laslett, G.M., Yoshida, H., and Olley, J.M., 1999, Optical dating of single and multiple grains of quartz from Jinmium Rock Shelter, northern Australia: Part 1. Experimental design and statistical models: Archaeometry, v. 41, p. 339–364, doi: 10.1111/j.1475-4754.1999.tb00987.x.

Hack, J.T., 1957, Studies of Longitudinal Stream Profiles in Virginia and Maryland: U.S. Geological Survey Professional Paper 294-B, p. 45–97.

Hancock, G.S., Anderson, R.S., and Whipple, K.X., 1998, Beyond power: Bedrock river incision process and form, *in* Tinkler, K.J., and Wohl, E.E., eds., Rivers over Rock: Fluvial Processes in Bedrock Channels: American Geophysical Union Geophysical Monograph 107, p. 35–60.

Hoth, S., Adam, J., Kukowski, N., and Oncken, O., 2006, Influence of erosion on the kinematics of bivergent orogens: Results from scaled sandbox simulations, *in* Willett, S.D., Hovius, N., Brandon, M.T., and Fisher, D.M., eds., Tectonics, Climate, and Landscape Evolution: Penrose Conference Series: Geological Society of America Special Paper 398, p. 201–225.

Howard, A.D., and Kerby, G., 1983, Channel changes in badlands: Geological Society of America Bulletin, v. 94, no. 6, p. 739–752, doi: 10.1130/0016-7606(1983)94<739:CCIB>2.0.CO;2.

Hsieh, M.L., and Knuepfer, P.L.K., 2001, Middle-late Holocene river terraces in the Erhjen River Basin, southwestern Taiwan—Implications of river response to climate change and active tectonic uplift: Geomorphology, v. 38, no. 3–4, p. 337–372, doi: 10.1016/S0169-555X(00)00105-7.

Johnson, K.M., Hsu, Y.J., Segall, P., and Yu, S.B., 2001, Fault geometry and slip distribution of the 1999 Chi-Chi, Taiwan earthquake imaged from inversion of GPS data: Geophysical Research Letters, v. 28, no. 11, p. 2285–2288, doi: 10.1029/2000GL012761.

Kirby, E., and Whipple, K., 2001, Quantifying differential rock-uplift rates via stream profile analysis: Geology, v. 29, no. 5, p. 415–418, doi: 10.1130/0091-7613(2001)029<0415:QDRURV>2.0.CO;2.

Kirby, E., Whipple, K.X., Tang, W.Q., and Chen, Z.L., 2003, Distribution of active rock uplift along the eastern margin of the Tibetan Plateau: Inferences from bedrock channel longitudinal profiles: Journal of Geophysical Research–Solid Earth, v. 108, no. B4, p. 1–24.

Lave, J., and Avouac, J.P., 2001, Fluvial incision and tectonic uplift across the Himalayas of central Nepal: Journal of Geophysical Research–Solid Earth, v. 106, no. B11, p. 26,561–26,591, doi: 10.1029/2001JB000359.

Lee, J.C., Chen, Y.G., Sieh, K., Mueller, K., Chen, W.S., Chu, H.T., Chan, Y.C., Rubin, C., and Yeats, R., 2001, A vertical exposure of the 1999 surface rupture of the Chelungpu fault at Wufeng, western Taiwan: Structural and paleoseismic implications for an active thrust fault: Bulletin of the Seismological Society of America, v. 91, no. 5, p. 914–929, doi: 10.1785/0120000742.

Liu, T.K., Hsieh, S., Chen, Y.G., and Chen, W.S., 2001, Thermo-kinematic evolution of the Taiwan oblique-collision mountain belt as revealed by zircon fission track dating: Earth and Planetary Science Letters, v. 186, no. 1, p. 45–56, doi: 10.1016/S0012-821X(01)00232-1.

Montgomery, D.R., and Gran, K.B., 2001, Downstream variations in the width of bedrock channels: Water Resources Research, v. 37, no. 6, p. 1841–1846, doi: 10.1029/2000WR900393.

Mueller, K.J., Chen, Y.G., and Keir, G., 2001, Erosion-induced backstepping and reaction of the Chelungpu thrust: Implications for the patterns of modern strain release in west-central Taiwan: Eos (Transactions, American Geophysical Union), v. 82, no. 47, T32A-0878, Fall meeting supplement, abstract.

Murray, A.S., and Wintle, A.G., 2000, Luminescence dating of quartz using an improved single-aliquot regenerative-dose protocol: Radiation Measurements, v. 32, no. 1, p. 57–73, doi: 10.1016/S1350-4487(99)00253-X.

Naylor, M., and Sinclair, H.D., 2007, Punctuated thrust deformation in the context of doubly vergent thrust wedges: Implications for the localization of uplift and exhumation: Geology, v. 35, no. 6, p. 559–562, doi: 10.1130/G23448A.1.

Pazzaglia, F.J., and Brandon, M.T., 2001, A fluvial record of long-term steady-state uplift and erosion across the Cascadia forearc high, western Washington State: American Journal of Science, v. 301, no. 4–5, p. 385–431, doi: 10.2475/ajs.301.4-5.385.

Powell, L.K., 2003, Feedback between Erosion and Fault Reactivation in the Puli Basin: Hsüehshan Belt of Central Taiwan [Master's thesis]: Boulder, Colorado, University of Colorado, 61 p.

Roe, G.H., Stolar, D.B., and Willett, S.D., 2006, Response of a steady-state critical wedge orogen to changes in climate and tectonic forcing, *in* Tectonics, Climate, and Landscape Evolution: Penrose Conference Taroko Gorge, Taiwan: Geological Society of America Special Paper 398, p. 227–239.

Selby, M.J., 1980, A rock mass strength classification for geomorphic purposes: With tests from Antarctica and New Zealand: Zeitschrift für Geomorphologie, v. 24, no. 1, p. 31–51.

Simoes, M., and Avouac, J.P., 2006, Investigating the kinematics of mountain building in Taiwan from the spatio-temporal evolution of the foreland basin and western foothills: Journal of Geophysical Research–Solid Earth, v. 111, no. B10, p. 1–25.

Simoes, M., Avouac, J.P., Beyssac, O., Goffe, B., Farley, K.A., and Chen, Y.G., 2007a, Mountain building in Taiwan: A thermokinematic model: Journal of Geophysical Research–Solid Earth, v. 112, no. B11, p. 1–25.

Simoes, M., Avouac, J.P., and Chen, Y.G., 2007b, Slip rates on the Chelungpu and Chushiang thrust faults inferred from a deformed strath terrace along the Dungpuna River, west central Taiwan: Journal of Geophysical Research–Solid Earth, v. 112, no. B3, p. 1–17.

Simoes, M., Avouac, J.P., Chen, Y.G., Singhvi, A.K., Wang, C.Y., Jaiswal, M., Chan, Y.C., and Bernard, S., 2007c, Kinematic analysis of the Pakuashan fault tip fold, west central Taiwan: Shortening rate and age of folding inception: Journal of Geophysical Research–Solid Earth, v. 112, no. B3, p. 1–30.

Snyder, N.P., Whipple, K.X., Tucker, G.E., and Merritts, D.J., 2000, Landscape response to tectonic forcing: Digital elevation model analysis of stream profiles in the Mendocino triple junction region, northern California: Geological Society of America Bulletin, v. 112, no. 8, p. 1250–1263, doi: 10.1130/0016-7606(2000)112<1250:LRTTFD>2.3.CO;2.

Snyder, N.P., Whipple, K.X., Tucker, G.E., and Merritts, D.J., 2003, Importance of a stochastic distribution of floods and erosion thresholds in the bedrock river incision problem: Journal of Geophysical Research–Solid Earth, v. 108, no. B2, p. 1–15.

Stark, C.P., 2006, A self-regulating model of bedrock river channel geometry: Geophysical Research Letters, v. 33, no. 4, p. 1–5, doi: 10.1029/2005GL023193.

Sung, Q.C., Chen, Y.C., Tsai, H., Chen, Y.G., and Chen, W.S., 2000, Comparison study on the coseismic deformation of the 1999 Chi-Chi earthquake and long-term stream gradient changes along the Chelungpu fault in central Taiwan: Terrestrial Atmospheric and Oceanic Sciences, v. 11, no. 3, p. 735–750.

Suppe, J., 2007, Absolute fault and crustal strength from wedge tapers: Geology, v. 35, no. 12, p. 1127–1130, doi: 10.1130/G24053A.1.

Tarboton, D.G., Bras, R.L., and Rodriguezituribe, I., 1989, Scaling and elevation in river networks: Water Resources Research, v. 25, no. 9, p. 2037–2051, doi: 10.1029/WR025i009p02037.

Tsai, H., and Sung, Q.C., 2003, Geomorphic evidence for an active pop-up zone associated with the Chelungpu fault in central Taiwan: Geomorphology, v. 56, no. 1–2, p. 31–47, doi: 10.1016/S0169-555X(03)00044-8.

Tucker, G.E., 2004, Drainage basin sensitivity to tectonic and climatic forcing: Implications of a stochastic model for the role of entrainment and erosion thresholds: Earth Surface Processes and Landforms, v. 29, no. 2, p. 185–205, doi: 10.1002/esp.1020.

Tucker, G.E., and Whipple, K.X., 2002, Topographic outcomes predicted by stream erosion models: Sensitivity analysis and intermodel comparison: Journal of Geophysical Research–Solid Earth, v. 107, no. B9, p. 1–16.

Turowski, J.M., Lague, D., and Hovius, N., 2007, Cover effect in bedrock abrasion: A new derivation and its implications for the modeling of bedrock channel morphology: Journal of Geophysical Research–Earth Surface, v. 112, no. F4, p. 1–16.

Upton, P., Mueller, K.J., and Chen, Y.G., 2009, Three dimensional numerical models with varied material properties and erosion rates: Implications for the mechanics and kinematics of compressive wedges: Journal of Geophysical Research–Solid Earth, v. 114, no. B04408, p. 1–18.

Wallinga, J., 2002, Optically stimulated luminescence dating of fluvial deposits: A review: Boreas, v. 31, no. 4, p. 303–322, doi: 10.1080/030094802320942536.

Whipple, K.X., 2004, Bedrock rivers and the geomorphology of active orogens: Annual Review of Earth and Planetary Sciences, v. 32, p. 151–185, doi: 10.1146/annurev.earth.32.101802.120356.

Whipple, K.X., and Meade, B.J., 2006, Orogen response to changes in climatic and tectonic forcing: Earth and Planetary Science Letters, v. 243, no. 1–2, p. 218–228, doi: 10.1016/j.epsl.2005.12.022.

Whipple, K.X., and Tucker, G.E., 1999, Dynamics of the stream-power river incision model: Implications for height limits of mountain ranges, landscape response timescales, and research needs: Journal of Geophysical Research–Solid Earth, v. 104, no. B8, p. 17,661–17,674, doi: 10.1029/1999JB900120.

Whipple, K.X., Hancock, G.S., and Anderson, R.S., 2000, River incision into bedrock: Mechanics and relative efficacy of plucking, abrasion, and cavitation: Geological Society of America Bulletin, v. 112, no. 3, p. 490–503, doi: 10.1130/0016-7606(2000)112<0490:RIIBMA>2.3.CO;2.

Whittaker, A.C., Cowie, P.A., Attal, M., Tucker, G.E., and Roberts, G.P., 2007, Bedrock channel adjustment to tectonic forcing: Implications for predicting river incision rates: Geology, v. 35, no. 2, p. 103–106, doi: 10.1130/G23106A.1.

Wilcox, T., Meuller, K.J., and Chen, Y.G., 2007, Systematic variations in synorogenic fill architecture and fault offsets along strike across the Puli topographic embayment: Quaternary strain gradients in the central Western Foothills and Taiwanese foreland basin, *in* Eos (Transactions, American Geophysical Union), v. 88, no. 52, Fall meeting supplement, abstract T32C–07.

Willett, S.D., 1999, Orogeny and orography: The effects of erosion on the structure of mountain belts: Journal of Geophysical Research–Solid Earth, v. 104, no. B12, p. 28,957–28,981, doi: 10.1029/1999JB900248.

Willett, S.D., and Brandon, M.T., 2002, On steady states in mountain belts: Geology, v. 30, no. 2, p. 175–178, doi: 10.1130/0091-7613(2002)030<0175:OSSIMB>2.0.CO;2.

Willett, S.D., Beaumont, C., and Fullsack, P., 1993, Mechanical model for the tectonics of doubly vergent compressional orogens: Geology, v. 21, no. 4, p. 371–374, doi: 10.1130/0091-7613(1993)021<0371:MMFTTO>2.3.CO;2.

Wobus, C., Whipple, K.X., Kirby, E., Snyder, N., Johnson, J., Spyropolou, K., Crosby, B., and Sheehan, D., 2006a, Tectonics from topography; procedures, promise, and pitfalls, *in* Tectonics, Climate, and Landscape Evolution: Penrose Conference Taroko Gorge, Taiwan: Geological Society of America Special Paper 398, p. 55–74.

Wobus, C.W., Tucker, G.E., and Anderson, R.S., 2006b, Self-formed bedrock channels: Geophysical Research Letters, v. 33, no. 18, p. 1–5, doi: 10.1029/2006GL027182.

Wobus, C.W., Kean, J.W., Tucker, G.E., and Anderson, R.S., 2008, Modeling the evolution of channel shape: Balancing computational efficiency with hydraulic fidelity: Journal of Geophysical Research–Earth Surface, v. 113, no. F2, p. 1–17.

Yanites, B.J., Tucker, G.E., Hsu, H.L., Chen, C.C., Chen, Y.G., Mueller, K.J., and Wilcox, T., 2008, Variability in hillslope sediment flux modulates bedrock channel incision rates: Evidence from the Peikang River, central Taiwan: Eos (Transactions, American Geophysical Union), v. 89, no. 53, Fall meeting supplement, abstract H54D-06.

Yue, L.F., Suppe, J., and Hung, J.H., 2005, Structural geology of a classic thrust belt earthquake: The 1999 Chi-Chi earthquake Taiwan (Mw=7.6): Journal of Structural Geology, v. 27, no. 11, p. 2058–2083.

Manuscript Received16 February 2009
Revised Manuscript Received 31 August 2009
Manuscript Accepted 4 September 2009

Printed in the USA